1983

Internal Rotation Effects and Nuclear Hyperfine Structure in the Microwave Spectrum of Propyne-HF

Roger E. Bumgarner
Eastern Illinois University

THESIS REPRODUCTION CERTIFICATE

TO: Graduate Degree Candidates who have written formal theses.

SUBJECT: Permission to reproduce theses.

The University Library is receiving a number of requests from other institutions asking permission to reproduce dissertations for inclusion in their library holdings. Although no copyright laws are involved, we feel that professional courtesy demands that permission be obtained from the author before we allow theses to be copied.

Please sign one of the following statements:

Booth Library of Eastern Illinois University has my permission to lend my thesis to a reputable college or university for the purpose of copying it for inclusion in that institution's library or research holdings.

12/1/83

Date Author

I respectfully request Booth Library of Eastern Illinois University not allow my thesis be reproduced because _____

_____

_____

_____ _____

Date Author

m

Internal Rotation Effects and Nuclear Hyperfine Structure in the Microwave Spectrum of Propyne-HF

(TITLE)

BY

Roger E. Bumgarner

THESIS

SUBMITTED IN PARTIAL FULFILLMENT OF THE REQUIREMENTS
FOR THE DEGREE OF

Master of Science in Chemistry

IN THE GRADUATE SCHOOL, EASTERN ILLINOIS UNIVERSITY
CHARLESTON, ILLINOIS

1983
YEAR

I HEREBY RECOMMEND THIS THESIS BE ACCEPTED AS FULFILLING
THIS PART OF THE GRADUATE DEGREE CITED ABOVE

11-29-83
DATE — ADVISER

11/29/83
DATE — COMMITTEE MEMBER

11/29/83
DATE — COMMITTEE MEMBER

11/29/83
DATE — DEPARTMENT CHAIRPERSON

Internal Rotation Effects and Nuclear Hyperfine Structure in the Microwave Spectrum of Propyne-HF

by

Roger E. Bumgarner
B.S. in Chemistry, May, 1982
Eastern Illinois University
Charleston, Illinois

Submitted in partial fulfillment
of the requirement for the degree of
Master of Science in Chemistry at the
Graduate School of Eastern Illinois University
Charleston, Illinois
1983

Table of Contents

Abstract

The microwave spectrum of the weakly bound propyne-HF/DF complex in the region between 6 and 16 GHz was analyzed. The spectrum was characteristic of a distorted T-shaped asymmetric top exhibiting torsional splitting caused by a low barrier to internal rotation of the methyl top relative to the propyne-HF frame. Deuterium substitution of HF confirms that the acid proton of HF is located between the F atom and the propyne triple bond. The spectroscopic constants given below are consistent with the fluorine atom being displaced toward the methyl group from a line perpendicular to and bisecting the propyne triple bond, suggesting a weak hydrogen bond interaction between fluorine and the methyl protons.

	Propyne-HF	Propyne-DF
A(MHz)	8722(9)	8644(12)
B(MHz)	3919(3)	3886(6)
C(MHz)	2753(1)	2728(2)
D_{aa}(kHz)	----	-23(6)
χ_{aa}(kHz)	----	163(6)
V_3(cm^{-1})	100(50)	100(50)

Acknowledgements

The author wishes to express his appreciation to Dr. Giles Henderson for many helpful and informative discussions on topics ranging from angular momentum to fishing, to maturity. Certainly more than just chemical physics was learned during my stay at Eastern.

The author also wishes to acknowledge J. A. Shea who, in conjunction with Dr. Giles Henderson, collected the data upon which this study was based.

List of Figures

List of Tables

INTRODUCTION

The microwave spectrum of the weakly-bound complex formed between propyne and HF has been recorded in the region between 6 and 16 GHz at the University of Illinois, by Dr. Giles L. Henderson and J. A. Shea, using a Flygare-Balle Spectrometer[1]. This study is an analysis of the above data to determine the structure and internal dynamics of the complex. This introduction is intended to serve the purpose of defining terms, briefly covering experimental methods of studying complexes (in particular the Flygare-Balle spectrometer), and reviewing the history of van der Waals complexes. Since the author did not directly participate in data collection or experimental design, no formal "Experimental Section" will follow.

It is necessary at this point to make a distinction between what will henceforth be called "weakly-bound complexes" and other molecules. The term "weakly-bound complex" shall refer to molecules composed of subunit molecules and/or atoms held together by intermolecular forces. The force between the two subunits will be referred to as "the weak bond." Weakly bound complexes can be classified as "classical van der Waals complexes" (Type I) and complexes composed of subunits containing one or more polar bonds (Type II). Type I complexes include molecules such as, $(Ne)_2$, H_2-Ar, $(Ar)_2$, N_2-Ar. Type II complexes include molecules such as $(CO_2)_2$, HCl-Ar, FCl-Ar, $(HF)_2$, C_2H_2-HF and propyne-HF. The main distinction between these types is that the subunits of Type I complexes are generally separated at equilibrium such that their van der Waals radii do not overlap, while in Type II complexes the van der Waals radii of the subunits penetrate each other. Table I. shows a comparison of bond parameters for typical chemical and weak bonds.

TABLE 1. Comparison of Bond Parameters for Chemical and Weak Bonds.

Parameter	Chemical Bond	Weak Bond
Stretching Force Constant (mdyne/Ang.)	1-22	.04-.6
Dissociation[a.] Energy (kJ/mol)	~340	~2.2
Temp. (K) at which the ave. kinetic energy of one molecule=De[a.]	~40,000	~270

a. Average over representative data set

Weakly-bound complexes have been the subject of a great deal of study and several texts and reviews have been written on the topic[2-8]. Weakly-bound complexes are important in explaining bulk properties of matter and they have been inferred as precursors in a variety of reaction mechanisms. Other phenomena which can be explained in terms of weakly-bound complexes includes spin-relaxation rates, nucleation and energy transfer mechansims. Many experimental methods of studying complexes take advantage of the effects described above. On the following pages, a few of these effects are described in more detail.

Equations of State

J. C. van der Waals was one of the earliest to suggest that deviations from ideal gas behavior could be accounted for on the basis of intermolecular forces. His famous equation of state

$$(P + an^2/V^2)\ (V - nb) = RT \qquad (1)$$

includes a pressure correction term, an^2/V^2, associated with intermolecular

forces and a volume correction term, -nb, acknowledging molecular volume or repulsive forces. Perhaps more generally useful is an expansion of his equation called the virial equation of state,

$$P = (RT/V_m) \{1 + B(T)/V_m + C(T)/V_m^2 + \ldots\}, \qquad (2)$$

where V_m is the molar volume. One can see that the major pressure correction term in this equation is B, the second virial coefficient. A negative B represents a decrease in pressure which could be attributed to the formation of weakly-bound complexes.

Table II. shows a comparison of measured values of (a) from the van der Waals equation and the temperature at which the second virial coefficient becomes negative, with the spectroscopically determined bond dissociation energy of the dimer for several gases. One can see a fairly general qualitative trend between De and (a), i.e. as (a) increases so does De. However, the relationship between De and the temperature at which the second virial coefficient becomes negative is more exact. In Figure 1., De is plotted vs. the temperature at which B(T) = 0. If CO_2 is excluded from the fit, an excellent straight line relationship (correlation coefficient = .994) is obtained. One should note that $(CO_2)_2$ is the only Type II. complex in the group. As expected, its dissociation energy is higher than that predicted by the relationship for Type I. complexes.

Phase Diagrams

Bulk properties of mixtures are also affected by complex formation. For example, the typical freezing point diagram for a mixture is shown in Figure 2a. However, if complex formation occurs, the freezing point

Table II. Comparison of Equation of State Parameters to Spectroscopically Determined Dissociation Energies for Dimer.

Gas	De (kJ/mol) of DIMER[a.]	a (dm^6 atm mol^{-2})[b.]	T(K) at which B(T) = 0[c.]
He	.07	.03142	22.64
Ne	.350	.2107	122.11
Ar	1.185	1.345	411.15
Kr	1.684	2.318	575.0
Xe	2.344	4.194	768.03
H_2	≳.29	.2444	111.04
N_2	.79	1.390	327.22
O_2	1.04	1.360	405.88
CO_2	1.6	3.592	346.81

a. Ref. 2.

b. Robert C. Weast, ed., "Handbook of Chemistry and Physics," 57th ed., p. D-178, Chemical Rubber Publishing Co., Cleveland, Ohio (1977).

c. Dwight E. Gray, ed., "American Institute of Physics Handbook," 3rd ed., pp. 4-(204-216), McGraw-Hill, New York, New York (1972).

Figure 1.

Plot of De vs. T at which B(T) = 0.

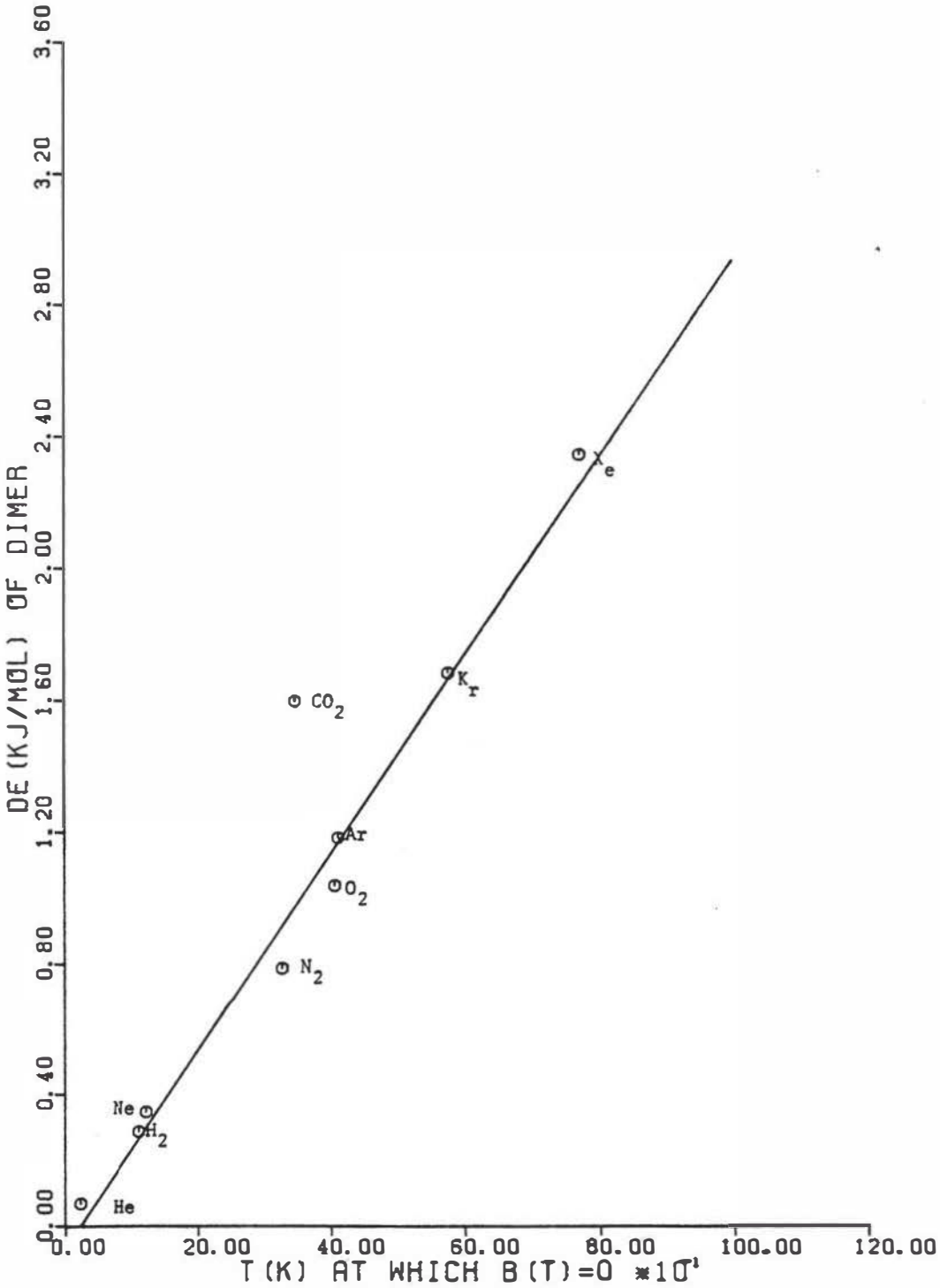
DE(KJ/MOL) OF DIMER
0.00
0.40
0.80
1.20
1.60
2.00
2.40
2.80
3.20
3.60
0.00
20.00
40.00
60.00
80.00
100.00
120.00
T(K) AT WHICH B(T)=0 *10¹
He
Ne
H2
N2
CO2
O2
Ar
Kr
Xe

Figure 2.

Freezing Point Diagram for:
a. A "Normal" Mixture
b. A Mixture Which Forms a Complex.

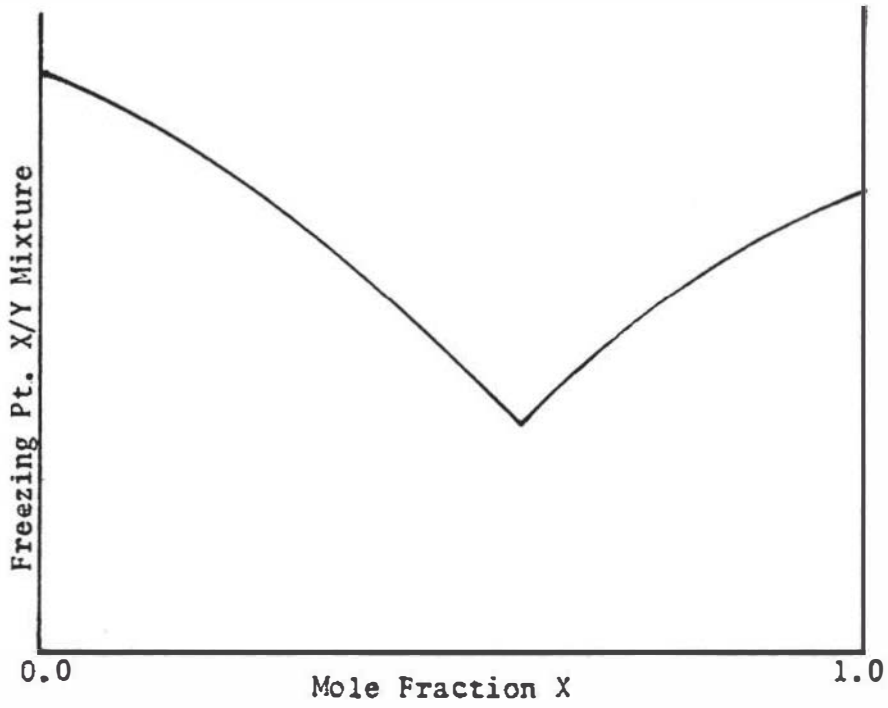
Freezing Pt. X/Y Mixture
0.0
Mole Fraction X
1.0

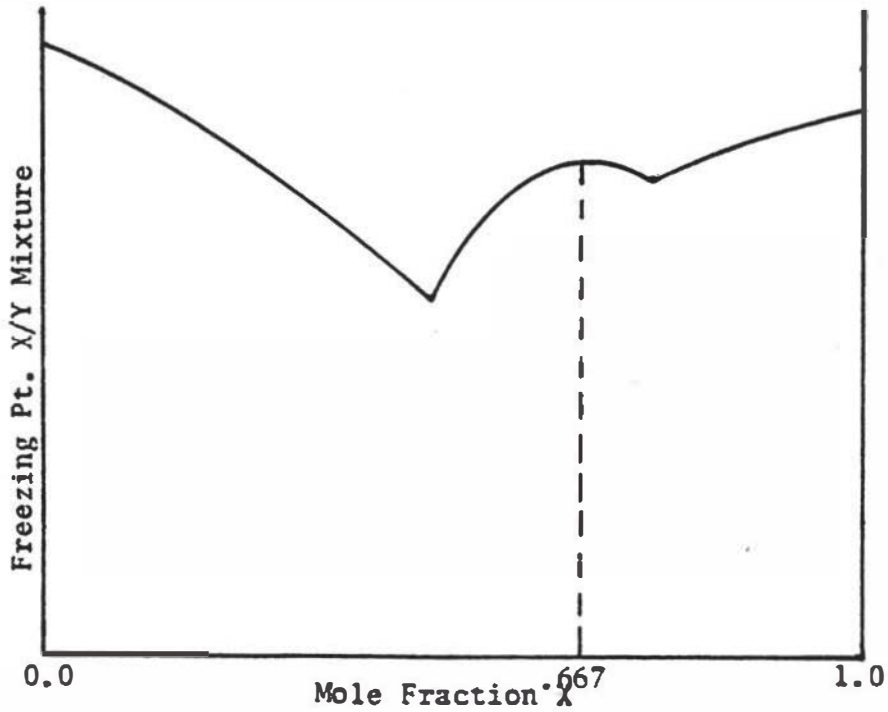
Freezing Pt. X/Y Mixture
0.0
.667
Mole Fraction X
1.0

diagram will show a maximum at the mixture ratio corresponding to the complex's subunit ratio as shown in Figure 2b. The maximum at $\overline{X} = .667$ corresponds to the formation of the X_2Y complex. Complex formation may also be indicated by negative deviations from Raoult's Law, a non-linear dependence of viscosity or refractive index on mole fraction, and a variety of other bulk property phenomena[a].

The above methods are all ways to infer complex formation. We shall now turn to methods of spectroscopically detecting weakly-bound complexes.

Equilibrium Spectroscopic Methods

The earliest spectroscopic studies of weakly-bound complexes were classical spectroscopy on equilibrium concentrations of complexes in the gas phase. The main complication of these methods is detecting low concentrations of complex. As indicated in Table I., the average weak bond will dissociate after one collision with a molecule at a mean translational temperature of ~270K. For systems at room temperature and one atmosphere, the time between collisions is on the order of 10^{-10} second and hence, the lifetime of a complex is comparable to 10^{-10} second.

These problems can be partially overcome by cooling the mixture. However, at low temperatures the gas may liquefy. At lower pressures the temperature of condensation will be lowered, but concentration will also decrease proportionally. Long path-length spectroscopy is the "brute-force" solution. However, larger cells require larger volumes of gas and are difficult to keep at thermal equilibrium. Several molecules have been studied by equilibrium methods including[3] $Ar-O_2$, HCl-Ar, Ar_2 and H_2-Ar.

---

a. Reference 8 contains numerous examples of these effects.

Non-Equilibrium Spectroscopic Methods

In order to overcome the problem of low concentrations of complexes in equilibrium mixtures, researchers have turned to non-equilibrium methods. The two principle methods are, isolation of complex in an inert gas matrix or production of complex in a molecular beam resulting from the expansion of a high pressure gas into a vacuum.

In the matrix isolation method, the components which are expected to form complexes are mixed, diluted with an inert gas and sprayed at a slow rate onto a CsI (or similar material) window which has been cooled to ~10K. Infrared is the usual spectroscopic source, although U.V.-Visible may also be used. Structural determinations of complexes isolated in a matrix are somewhat suspect since the matrix applies a perturbation to the complex it contains. Complexes studied in this manner include CH_3F-HF[9], HCN-HF[10] and C_2H_2-HF[11]. To obtain accurate structural determinations rotational spectroscopy is the method of choice if detectable populations of complexes can be prepared in the gas phase. Two different methods have been developed to obtain rotational spectra from molecular beams of complexes.

William Klemperer and associates have adopted the technique of molecular beam electron resonance spectroscopy (MBER)[12, 13]. Their spectrometer consists of a molecular beam source of complexes which passes through two non-uniform electrostatic quadrupole fields separated by an intermediate resonance region followed by a 60° sector mass spectrometer as a detector. A deflecting force which is dependent on field strength, field gradient and effective molecular dipole acts upon the beam in both fields. Since effective molecular dipole is dependent on quantum state, the two field regions can be chosen in strength, gradient, and length such that the second field will exactly counteract the deflection of the first field for only one

particular quantum state. Hence, a particular quantum state can be focused onto the entrance slit of a mass spectrometer. The intermediate resonance region is then interrogated at either microwave or radio frequencies and absorptions are detected as a decrease in beam intensity. Stark experiments may also be performed by applying a homogeneous field across the resonance region.

The main advantage of this method is the use of a mass spectrometer as a detector. This provides high sensitivity detection if at least one fragment of the complex under study has a unique charge to mass ratio relative to other mixture components. Also since masses are determined directly, there is usually little doubt as to the composition of the complexes under study.

Flygare and co-workers have developed the method of pulsed nozzle, Fourier-transform microwave spectroscopy[14-17]. A schematic of their instrument is shown in Figure 3. A short pulse (~3 msec) of a gas mixture is expanded supersonically into a Fabrey-Perot cavity. Adiabatic cooling produces a mixture rich in complexes with effective rotational temperatures of ~5K. After a few milliseconds delay, a pulse of microwave energy enters the cavity through the pin diode switch in line after the master oscillator. The pulse is adjusted in power and duration to produce maximum sample polarization. After a short delay (~.1μs) to allow the polarizing radiation to dissipate, the coherent free induction decay from all the rotational frequencies within the bandwidth of the cavity is mixed down, detected with a superheterodyne receiver, digitized and stored. After the gas has been evacuated, a background signal is obtained and subtracted from the original signal. The process is repeated and the signals are averaged over a suitable number of pulses. The final signal is then Fourier transformed to the frequency domain power spectrum.

Figure 3.

Schematic Diagram of the Flygare-Balle Spectrometer.

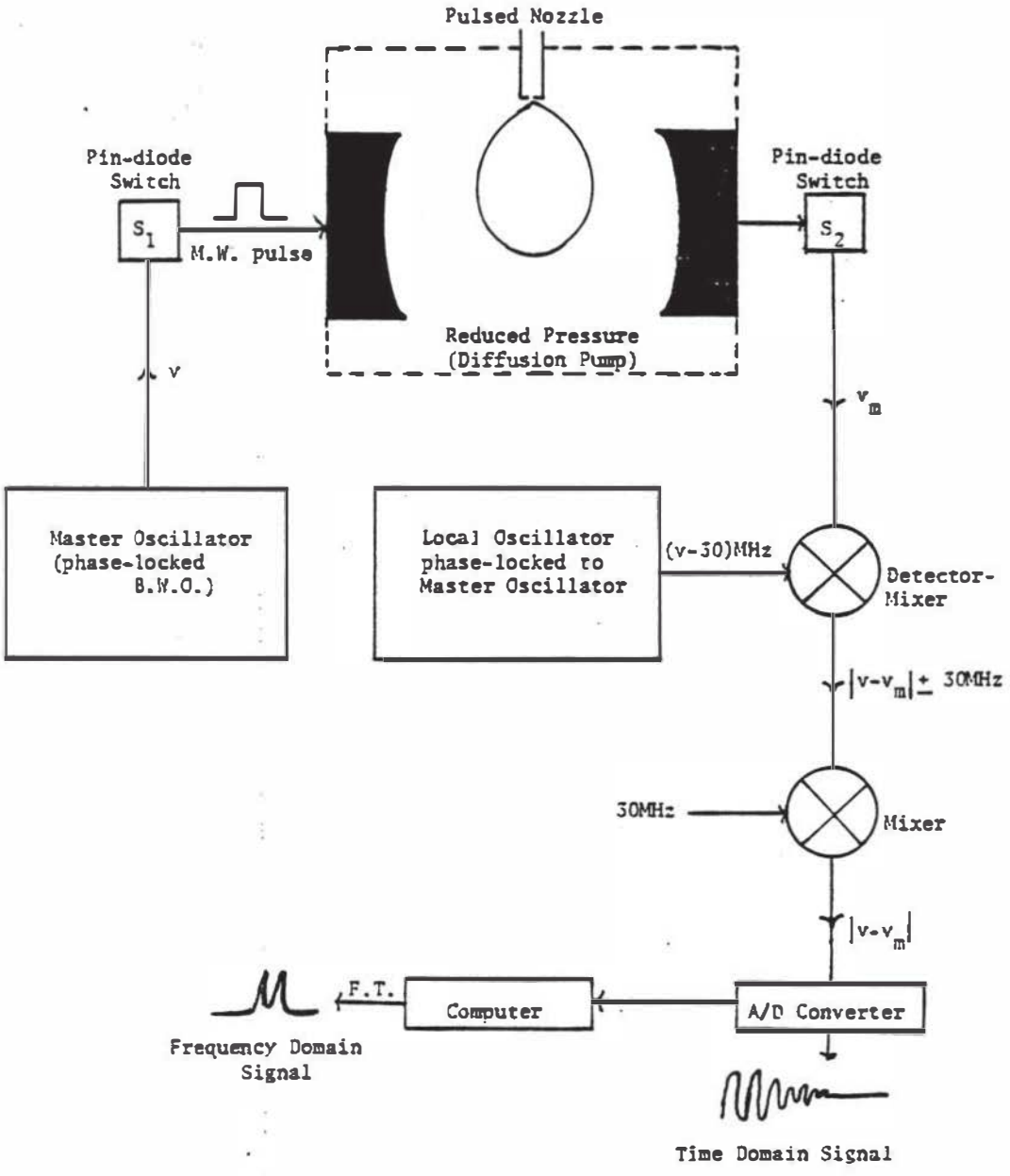
Pulsed Nozzle
Pin-diode Switch
S_1
M.W. pulse
Pin-diode Switch
S_2
Reduced Pressure (Diffusion Pump)
ν
ν_m
Master Oscillator (phase-locked B.W.O.)
Local Oscillator phase-locked to Master Oscillator
(v-30)MHz
Detector-Mixer
$|\nu-\nu_m| \pm 30$MHz
30MHz
Mixer
$|\nu-\nu_m|$
F.T.
Computer
A/D Converter
Frequency Domain Signal
Time Domain Signal

The main advantages of this technique is the inherent sensitivity of Fourier transform spectroscopy and high resolution (~10kHz on their spectrometer). The method has also been recently extended to allow measurement of Stark and Zeeman spectra[14-15].

Appendix 1. contains a table of selected properties of many known weakly bound complexes along with an indication of the method(s) of study and appropriate references.

Theory

The data obtained consists of the microwave spectrum of Propyne-HF/DF recorded in the region between 6 and 16 GHz with a resolution of ~10 kHz. The theory used to interpret these data consists of: the theory of the rigid asymmetric rotor, the theory of the asymmetric rotor containing a rigid internal rotor, and the theory of nuclear hyperfine structure. In the following sections each of these theories is described separately and a sample spectrum is provided at each level of theory. Since both methanol and propyne-HF/DF are near prolate, a-dipole asymmetric rotors with low barrier internal rotation of a C_3 top, methanol is used as the example in the rigid rotor and internal rotation sample spectra.

Rigid Rotor[a.]

The classical Hamiltonian for a rigid rotating top in its principal frame can be written as follows,

a. This section is intended to serve as a brief overview of the rigid rotor. Many textbook discussions are available. See, for example, Ref. 16.

$$H = \frac{J_a^2}{2I_{aa}} + \frac{J_b^2}{2I_{bb}} + \frac{J_c^2}{2I_{cc}} \qquad (3)$$

where J_g and I_{gg} are the angular momentum and moment of inertia about the g axis. The matrix representation of the Hamiltonian in the prolate basis is[19]

$$\langle JKM|H_{RR}|JK\rangle = \frac{h(B+C)}{2}[J(J+1)-K^2]+hk^2A \qquad (4)$$

$$\langle JKM|H_{RR}|JK\pm2M\rangle = \frac{h}{4}(B-C)[J(J+1)-K(K\pm1)]^{\frac{1}{2}}[J(J+1)-(K\pm1)(K\pm2)]^{\frac{1}{2}} \qquad (5)$$

where

$$A = \frac{\hbar^2}{4\pi I_{aa}}, \quad B = \frac{\hbar^2}{4\pi I_{bb}} \quad \text{and} \quad C = \frac{\hbar^2}{4\pi I_{cc}}$$

These equations can be permuted to the oblate case by the following[19]

prolate → oblate

A → C

B → A

C → B

The above matrix may be diagonalized to yield the energy levels of the asymmetric rigid rotor. Alternatively, for low J states, one may use the reduced energy expressions as derived by King, Hainer and Cross[20]. Energy levels of the asymmetric rotor are labeled $J_{K_{-1}K_{+1}}$, where K_{-1} and K_{+1} correspond to the K quantum numbers in the prolate and oblate limits. J selection rules for transitions between energy levels are $\Delta J=0, \pm1$. K selection rules, which depend upon the projection of molecular dipole on the principal axes are given in Table III. Figure 4. shows a plot of the a-dipole rigid rotor spectrum of a near prolate top.

Figure 4.

Rigid Rotor Spectrum of CH_3OH A=127532 MHz, B=24672.5 MHz
C=23762.5 MHz.

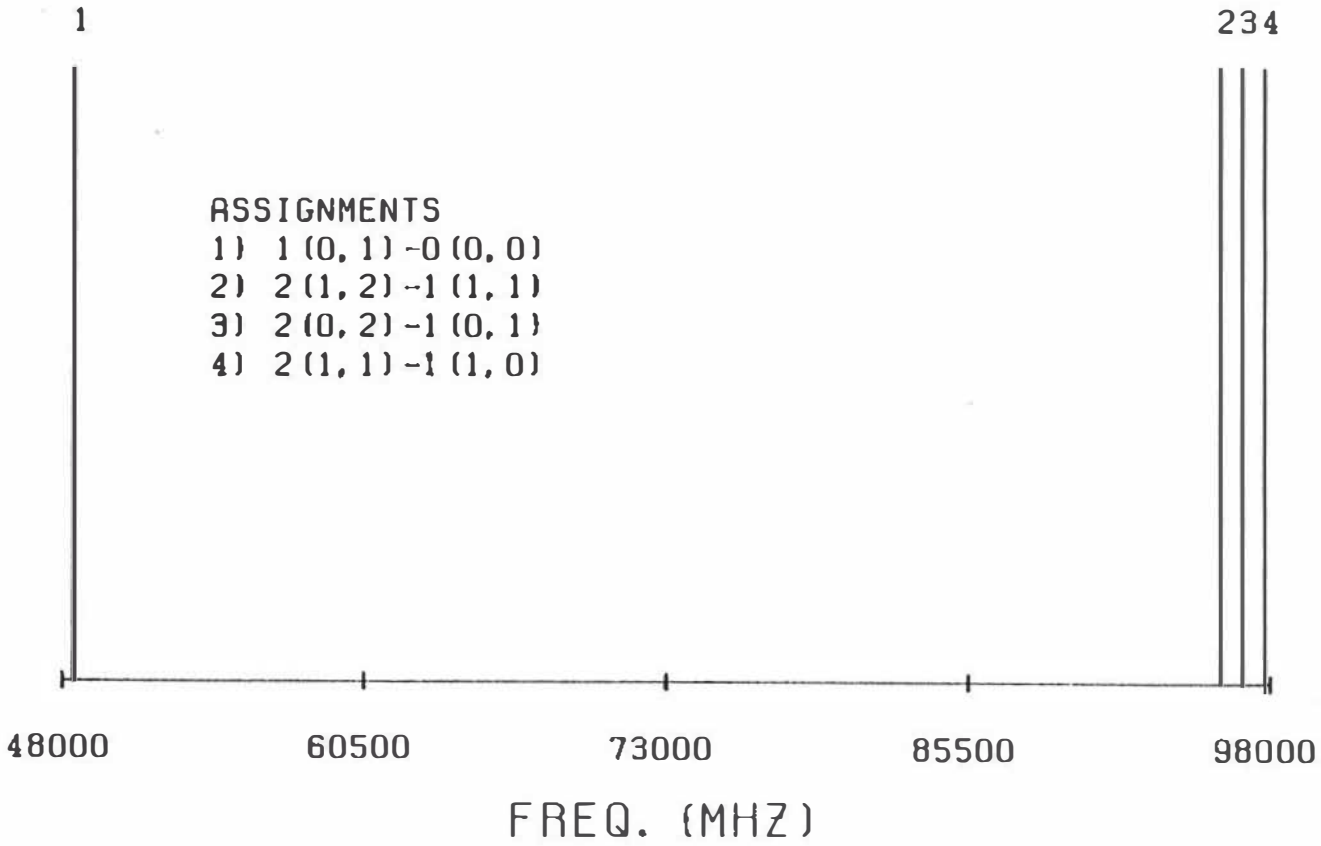
1
234
ASSIGNMENTS
1) 1 (0, 1) -0 (0, 0)
2) 2 (1, 2) -1 (1, 1)
3) 2 (0, 2) -1 (0, 1)
4) 2 (1, 1) -1 (1, 0)
48000
60500
73000
85500
98000
FREQ. (MHZ)

Table III. K-selection Rules for an Asymmetric Rigid Rotor. The notation of (e) and (o) refers to the evenness and oddness of the K quantum numbers.

Allowed Transitions		
a-dipole	b-dipole	c-dipole
ee ↔ eo	oo ↔ ee	ee ↔ oe
oo ↔ oe	eo ↔ oe	eo ↔ oo

Rigid Rotor - Rigid Hindered Internal Rotor

If subunits within a molecule rotate with respect to each other, there exists a projection of angular momentum on the principal axes due to this internal rotation. The classical Hamiltonian for the rotational energy of a molecule with one internal rotor as developed by Crawford[21] is

$$H = H_{RR} + F(p-P)^2 + (Vm/2)(1-\cos m\alpha) \tag{6}$$

where

$$F = \hbar^2/2rI_\alpha, \tag{7}$$

$$r = 1 - \sum_g I_\alpha \lambda_g^2 / I_g \qquad g = x,y,z, \tag{8}$$

$(p - P)$ is the operator describing the relative angular momentum of the top and the frame, λ_g is the direction cosine of the top axis with the g principal axis, I_α is the moment of inertia of the top about its axis of internal rotation, V_m is the height of the m periodic barrier and α is the relative angle of the top with the frame. The first term in equation 6 is the usual rigid rotor Hamiltonian, representing the kinetic energy due

to overall rotation of the molecule. The second term represents the additional kinetic energy due to the internal top rotating relative to the frame. The third term represents the potential energy the internal top experiences in rotating relative to the frame. For a top in a force field of C_3 symmetry, the potential energy is written as

$$P.E. = (V_3/2)(1-\cos 3\alpha). \tag{9}$$

Figure 5. shows a plot of this potential function and the definition of α. Since propyne-HF contains a methyl top as its internal rotor, the following internal rotor discussion is specific to a top in a force field of C_3 symmetry.

Since a low barrier was expected in this case, the matrix elements of equation 6 were derived in the prolate symmetric top-free rotor basis. These matrix elements have been correctly derived previously[22] but, since conflicting expressions can be found in the literature[23], they were re-derived during this study. An outline of the derivation can be found in Appendix 2. The non-zero elements are:

$$\langle JKMm|H|JKMm\rangle = [(B+C+F\beta^2+F\gamma^2)/2][J(J+1)-K^2]+(\alpha^2F+A)K^2+Fm^2-2m\alpha K+V_3/2 \tag{10}$$

$$\langle JKMm|H|JKMm\pm 3\rangle = -V_3/4 \tag{11}$$

$$\langle JKMm|H|JK\pm 1Mm\rangle = (\tfrac{1}{2})F[\alpha(2K\pm 1)-2m]-(\beta\pm i\gamma)[J(J+1)-K(K\pm 1)]^{\frac{1}{2}} \tag{12}$$

$$\langle JKMm|H|JK\pm 2Mm\rangle = (\tfrac{1}{4})[C-B+F(\beta\pm i\gamma)^2][J(J+1)-K(K\pm 1)]^{\frac{1}{2}}[J(J+1)-(K\pm 1)(K\pm 2)]^{\frac{1}{2}} \tag{13}$$

where

$$\alpha = \lambda_z I_\alpha / I_z, \quad \beta = \lambda_x I_\alpha / I_x \quad \text{and} \quad \gamma = \lambda_y I_\alpha / I_y. \tag{14}$$

Since the basis set wave functions can be classified as either E or A symmetry under the operations of the D_3 point group, matrix diagonalization may be greatly facilitated by symmetry block factoring. Also, for

Figure 5.

Plot of the Barrier Potential Function and Definition of α.

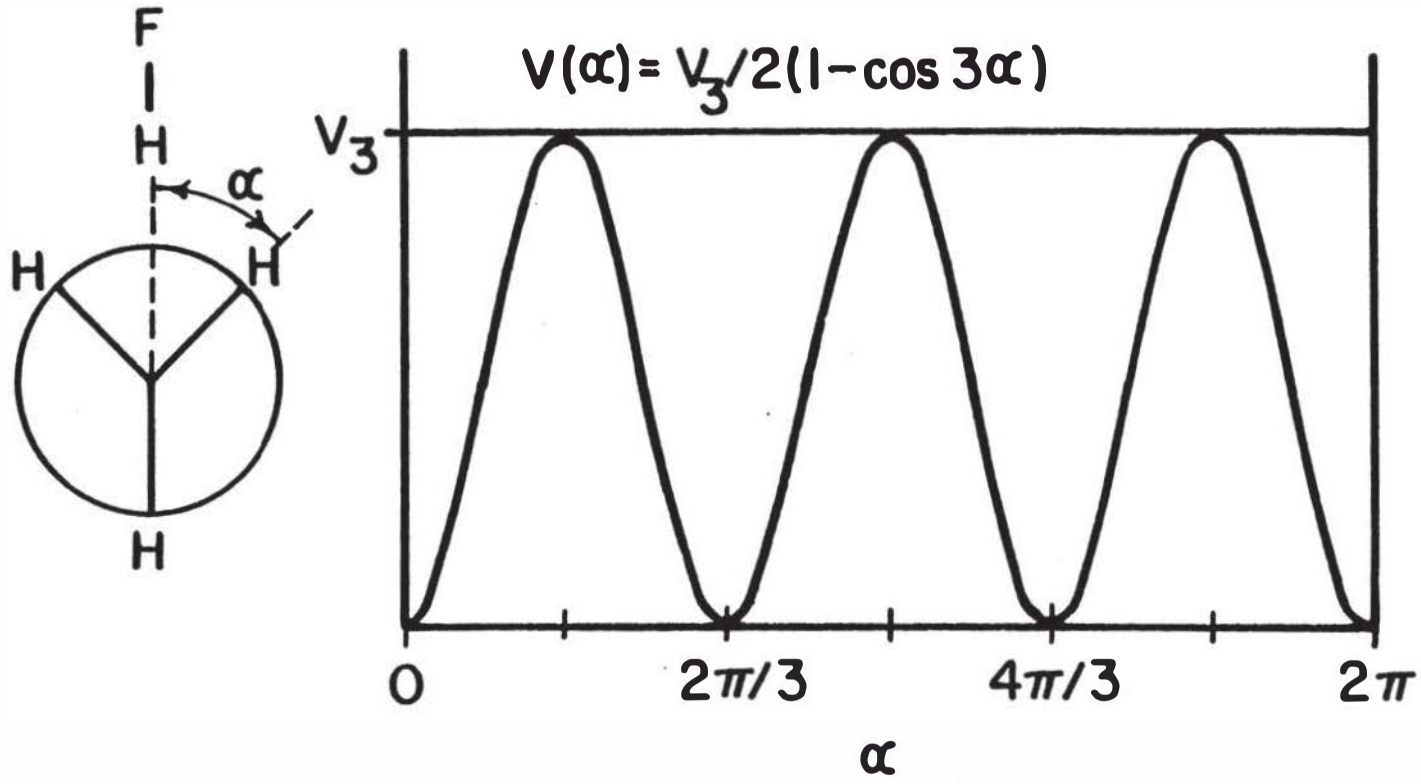
F
H
H
α
H
H
H
V(α)= V3/2(1−cos 3α)
V3
0
2π/3
4π/3
2π
α

molecules with a plane of symmetry, the A wave functions can be factored into degenerate A_1 and A_2 blocks. In practice, for coding simplicity, only A-E block factoring was applied. This corresponds to A states of m=0 mod 3 and degenerate E states of m=±1 mod 3.

Figure 6. shows a correlation diagram for the internal energy levels between the free rotor and harmonic librator limits. Energy levels are classified according to the symmetry of the wave functions from which they were derived. The dipole selection rule is $\Delta m=0$. Figure 7. shows the spectrum of methanol calculated using the above model and assuming that only the lower energy levels (i.e. those corresponding to m=0 in the free rotor limit) are populated. The parameters used in this calculation are recorded in Table IV.

Table IV. Spectroscopic and Structural Parameters of CH_3OH[24].

$A(MH_3)$	127532
$B(MH_3)$	24672.6
$C(MH_3)$	23762.5
V_3(cm-1)	375.6
λ_x	.05364
λ_z	.998520
λ_y	0 (methyl top is in X-Z plane)
I_α(Amu-Å^2)	3.21321

Nuclear Hyperfine

The nuclear interactions responsible for hyperfine which must be considered are spin-spin and nuclear quadrupole. The spin-spin Hamiltonian

Figure 6.

Correlation Between the Free Rotor (V_3=0) and High Barrier (V_3=∞) Energy Levels.

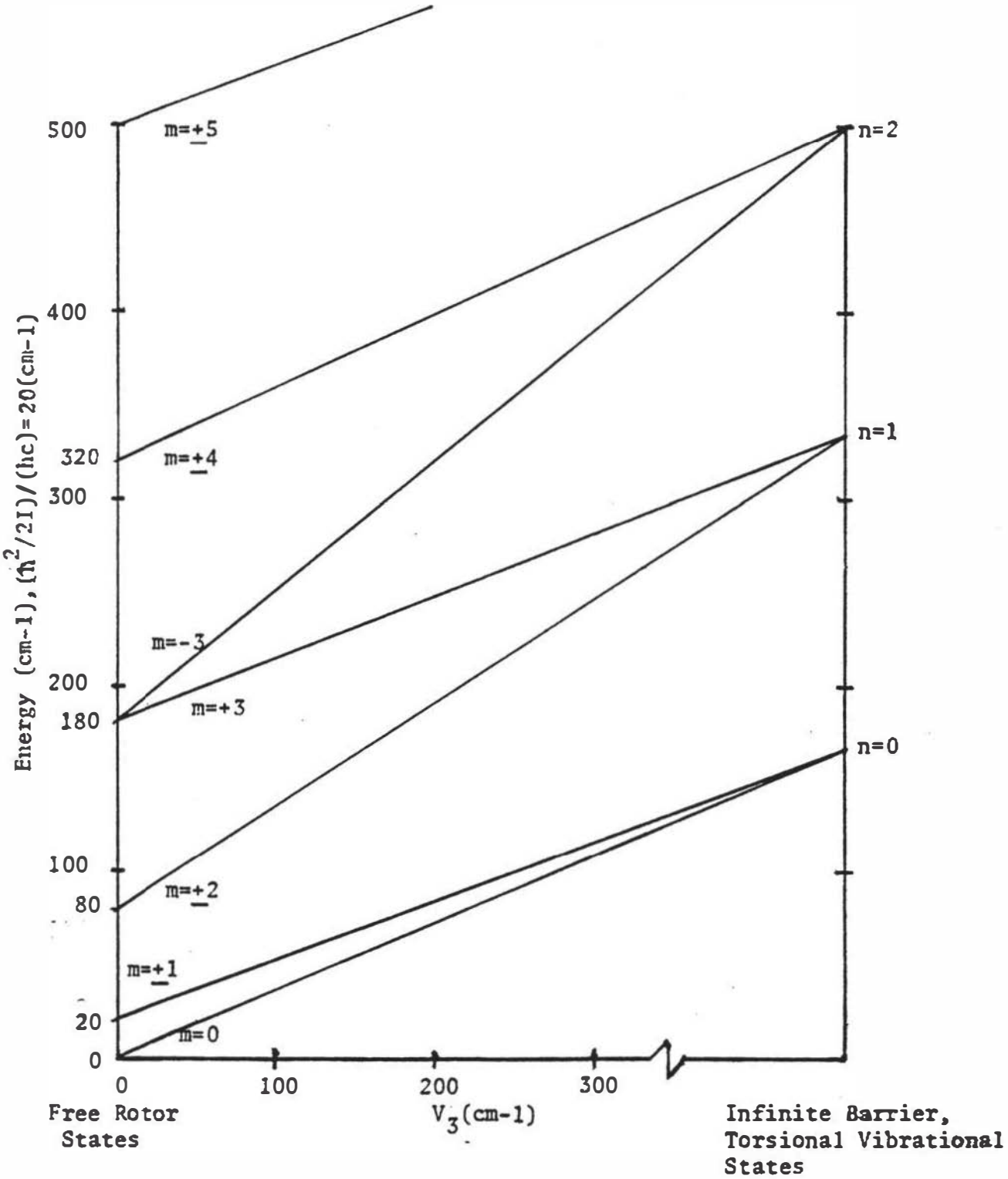
500
400
320
300
200
180
100
80
20
0
Energy (cm-1), $(\hbar^2/2I)/(hc) = 20$(cm-1)
m=±5
m=±4
m=-3
m=+3
m=±2
m=±1
m=0
n=2
n=1
n=0
0
100
200
300
V_3(cm-1)
Free Rotor States
Infinite Barrier, Torsional Vibrational States

Figure 7.

Plot of CH_3OH Spectrum Calculated Using Hindered Internal Rotor Model.

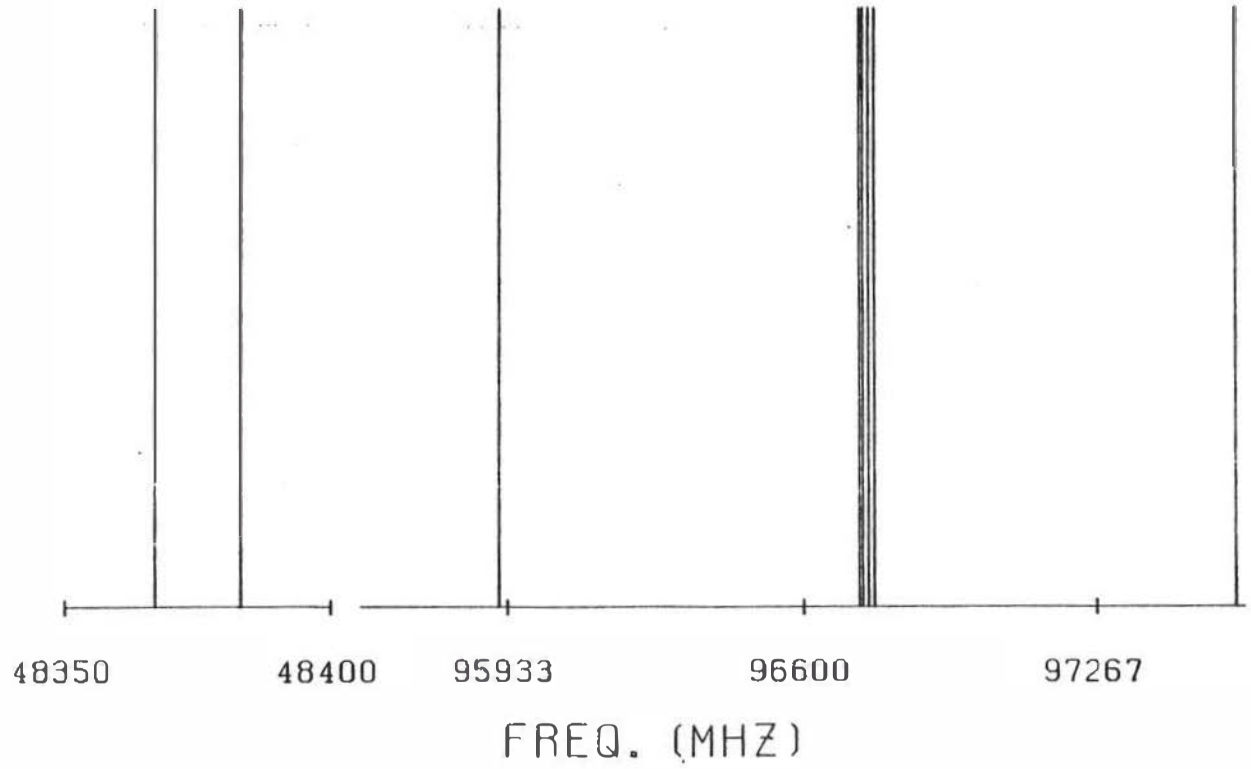
48350
48400
95933
96600
97267
FREQ. (MHZ)

can be written as the classical interaction between two magnetic dipoles[26]:

$$H_{ss} = \frac{1}{R^3}\{\mu_1 \cdot \mu_2 - 3(\mu_1 \cdot R)(\mu_2 \cdot R)/R^2\} \tag{15}$$

where R is a vector from nucleus 1 to nucleus 2. μ_i is the nuclear magnetic moment due to nuclear angular momentum $\underset{\sim}{I}_i$ and can be expressed as

$$\mu_i = \mu_N g_i \underset{\sim}{I}_i \tag{16}$$

where μ_N is the nuclear magneton and g_i is the nuclear g value for the i^{th} nucleus, Substitution of equation 16 into equation 15 yields

$$H_{ss} = \underset{\sim}{I}_F \cdot \underset{\approx}{D} \cdot \underset{\sim}{I}_{H/D} \tag{17}$$

where $\underset{\approx}{D}$ is the spin-spin coupling tensor with elements given by

$$D_{ij} = \frac{g_F g_{H/D} \mu_N^2 (R_2 \delta_{ij} - 3R_i R_j)}{R^5} \tag{18}$$

$$i,j - x,y,z.$$

The nuclear quadrupole interaction is given by:

$$H_q = \underset{\approx}{Q}(D) : \underset{\approx}{V}(D) \tag{19}$$

where $\underset{\approx}{Q}(D)$ and $\underset{\approx}{V}(D)$ are the deuterium nuclear quadrupole coupling and electric field gradient tensors respectively. The total Hamiltonian is simply

$$H = H_R + H_{ss} + H_q. \tag{20}$$

The matrix elements of equations 17 and 19 have been derived[25,27] on the basis:

$$I_F + I_{H/D} = I, \quad I + J = F. \tag{21}$$

They are:

$$\langle I_F I_{H/D} IJKFM | H_{ss} | I_F I_{H/D} I'J'K'I'M \rangle = \delta_{FF'}\delta_{MM'}(-1)^{F+K+I'} \cdot$$

$$[30(2I+1)(2I'+1)(2I_F+1)(I_F+1)I_F(2I_{H/D}+1)(I_{H/D}+1)I_{H/D}(2J+1)(2J'+1)]^{\frac{1}{2}} \cdot$$

$$\begin{pmatrix} J & 2 & J' \\ -K & -q & K' \end{pmatrix} \begin{Bmatrix} I & I' & 2 \\ J' & J & F \end{Bmatrix} \begin{Bmatrix} I_F & I_F & 1 \\ I_{H/D} & I_{H/D} & 1 \\ I & I & 2 \end{Bmatrix} \quad \frac{D^{2'}_{-q}}{2} \tag{22}$$

and

$$\langle I_F I_D IJKM | H_q | I_F I_D I'J'F'M' \rangle = \delta_{FF'}\delta_{MM'} \frac{(-1)^{I'+I_F+I_D+F+K}}{4} \cdot$$

$$[(2I+1)(2I'+1)(2J+1)(2J'+1)]^{\frac{1}{2}} \begin{Bmatrix} I & I' & 2 \\ J' & J & F \end{Bmatrix} \begin{pmatrix} J & 2 & J' \\ -K & -q & K' \end{pmatrix} \cdot$$

$$(-1)^I \frac{\begin{Bmatrix} I & I' & 2 \\ I_D & I_D & I_F \end{Bmatrix}}{\begin{pmatrix} I_D & 2 & I_D \\ -I_D & 0 & I_D \end{pmatrix}} \left(\chi_{2-q}\right)_D \tag{23}$$

where $q=K'-K$, the six membered quantities in parenthesis and braces are 3-j and 6-j symbols respectively and the nine membered quantity in braces a 9-j symbol. $D2'-q$ and χ_{2-q} are spherical tensors in the molecular axis frame and are related to the cartesian tensors by

$$D^{2'}_{o} = D_{aa} \tag{24}$$

$$D^{2'}_{\pm 1} = \mp(2/3)^{\frac{1}{2}}(D_{ba} \pm iD_{aa}) \tag{25}$$

$$D^{2'}_{\pm 2} = (1/6)^{\frac{1}{2}}(D_{bb} - D_{cc} \pm 2iD_{BC}) \tag{26}$$

$$\chi_{20} = \chi_{aa} \tag{27}$$

$$\chi_{2\pm1} = \pm(2/3)^{\frac{1}{2}}\chi_{ab} \tag{28}$$

and $$\chi_{2\pm2} = (1/6)^{\frac{1}{2}}(\chi_{bb}-\chi_{cc}). \tag{29}$$

Subroutines to evaluate 3j, 6j and 9-j symbols were kindly provided by J. A. Shea. Figure 8 shows a plot of the hyperfine pattern of the J=0-1 transitions for acetlyne-HF/DF[25].

Method and Results

The data obtained consist of the J=0-1 and J=1-2 transitions of propyne-HF/DF. These transitions, as recorded, exhibit torsional splittings, nuclear hyperfine and Doppler splitting due to the gas dynamics. Due to the low rotational temperatures of the expanding gas, only the torsional states corresponding to m=0 (A) and m=±1 (E) in the free rotor limit were observed[a]. The frequency averaged line centers of both the A and E symmetry states along with their assignments are reported in Table V. Since E symmetry torsional states are of higher energy than corresponding A symmetry lines, symmetry assignments were made on the basis of observed intensities, i.e. lines assigned as transitions between E symmetry states were of markedly lower intensity than those assigned as A symmetry transtions. It was not possible to confidently assign K-prolate/K-oblate quantum numbers to the J=1-2 symmetry lines.

Since m is the quantum number characterizing the free rotor basis and hence, the relative angular momentum of the top, one might expect that the A symmetry lines are least perturbed by internal rotation effects.

a. Henceforth the terms A and E symmetry shall be understood to mean the states corresponding to m=0 and m=±1 in free rotor limit, respectively.

Figure 8.

$0_{oo} \rightarrow 1_{01}$ Hyperfine Pattern of C_2H_2-DF[25].

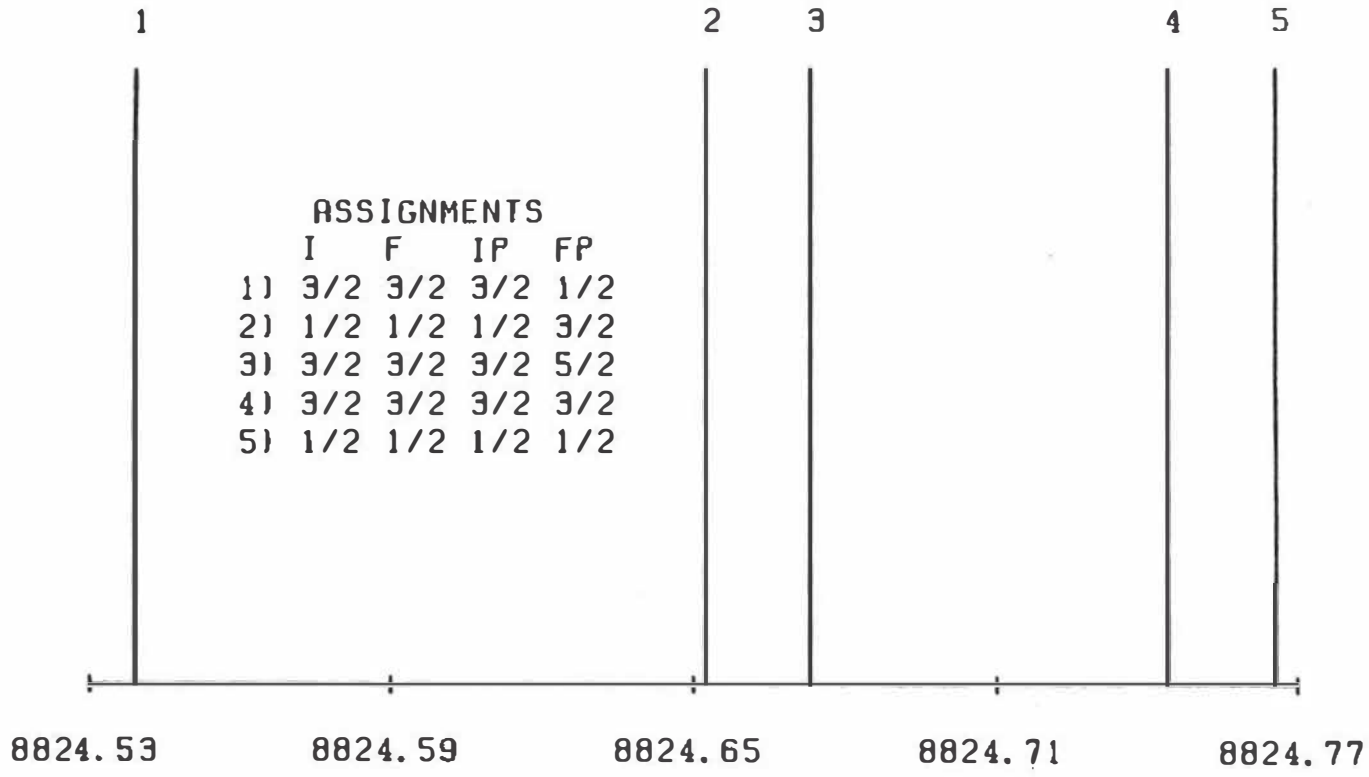
1
2
3
4
5
ASSIGNMENTS
I F IP FP
1) 3/2 3/2 3/2 1/2
2) 1/2 1/2 1/2 3/2
3) 3/2 3/2 3/2 5/2
4) 3/2 3/2 3/2 3/2
5) 1/2 1/2 1/2 1/2
8824.53
8824.59
8824.65
8824.71
8824.77
FREQ. (MHZ)

Table V. Frequency Averaged Line Centers (MHz).

	Propyne-HF		Propyne-DF	
	Observed	Calculated	Observed	Calculated
0(0,0)-1(0,1)A	6714.26	6697.19	6652.25	6639.57
0(0,0)-1(0,1)E	6755.28	---	6724.79	---
1(1,1)-2(1,2)A	12224.82	12252.47	12121.96	12146.27
1(0,1)-2(0,2)A	13242.91	13214.04	13126.02	13099.93
1(1,0)-2(1,1)A	14525.41	14536.21	14402.87	14411.93
1-2 E	13164.73	---	13066.36	---
1-2 E	13186.98	---	13092.56	---
1-2 E	13199.55	---	13148.63	---

Indeed, these lines exhibit a pseudo-rigid rotor spectrum and may be analyzed to obtain effective rigid rotor rotational constants as follows. Formulas for frequencies of the J=0-1 and J=1-2 rigid rotor transitions are provided in Table VI.

Table VI. Rigid Rotor Transition Frequencies for a Near Prolate Assymmetric Rotor[16].

Transition	Frequency
$0_{oo} \rightarrow 1_{01}$	B+C
$1_{11} \rightarrow 2_{12}$	B+3C
$1_{01} \rightarrow 2_{02}$	$2A+B+C-2[(B-C)^2+(A-C)(A-B)]^{\frac{1}{2}}$
$1_{10} \rightarrow 2_{11}$	3B+C

As one can see, the frequency difference between the $1_{11} \rightarrow 2_{12}$ and $1_{10} \rightarrow 2_{11}$ lines is equal to 2(B-C). Hence, this frequency difference and the $0_{oo} \rightarrow 1_{01}$ line yield simultaneous equations which can be solved for B and C. These values of B and C, along with the frequency of the $1_{01} \rightarrow 2_{02}$ line, can be used to calculate A. Since internal rotation is neglected, the constants obtained in this method must be regarded as effective rotational constants. The values obtained are recorded in Table VII.

A structure was fit, using the Jacobi least-squares method, to the effective rigid rotor constants calculated about with the following two assumptions: (1) the structures of the monomers (Table VIII) were assumed to remain unchanged upon complexation and (2) the F → H vector of HF was assumed to bisect the triple bond of propyne. The first assumption is a usual assumption made for weakly-bound complexes and a great deal of

---

a. A copy of the least squares program used is in Appendix 3.

Table VII. Spectroscopic and Structural Parameters of the Complex[a].

	Pseudo-Rigid Rotor[b]		Hindered Internal Rotor	
	Propyne-HF	Propyne-DF	Propyne-HF	Propyne-DF
A(MHz)	8722(9)	8644(12)	8657	8747
B(MHz)	3919(3)	3886(6)	3932	3896
C(MHz)	2753(1)	2728(2)	2782	2756
R_F(Ang.)	3.07(3)	3.08(2)	3.07(1)	3.06(1)
β(dg)	82(3)	81(3)	81(1)	82(1)
D_{aa}(kHz)	---	---	---	-23(6)
χ_{aa}(kHz)	---	---	---	163(6)
γ*(deg)[c]	---	---	---	34(6)
γ*(deg)[d]	---	---	---	37(1)

[a] Values in parentheses represent one standard deviation in the fit.

[b] Effective constants.

[c] Determined from D_{aa}.

[d] Determined from χ_{aa}.

Table VIII. Monomer Structures and Molecular Constants.

	Propyne[a]	HF	DF
Bond Lengths and Structural Parameters	<HCH=108°25' <HCC=110°30' R(CH,Me)=1.1124Å R(CH,Acyl)=1.0602Å R(C-C)=1.4577Å R(C≡C)=1.2073Å	R_o=.925595Å	R_o=.92326Å[f]
Rotational Constants (MHz)	B_o=8545.8691[b]	B_o=616365.5[c]	B_o=325584.98[d]
D_o (kHz)	----	-286.75[e]	-44.340[e]
χ(D) (kHz)	----	----	354.283[e]
I_α(Amu-Å^2)	3.2822	----	----

[a] L. F. Thomas, E. I. Sherrard, and J. Sheridan, Trans. Faraday Soc. 51, 619 (1955).

[b] A. Bauer and J. Burie, Compt. Rendu 268B, 800 (1969).

[c] G. Guelachvili, Opt. Commun. 19, 150 (1976).

[d] F. J. Lovis and E. Tiemann, J. Phys. Chem. Ref. Data 3, 397 (1974).

[e] J. S. Muenter, J. Chem. Phys. 56, 5409 (1972).

[f] F. C. DeLucia, P. Helminger and W. G. Gordy, Phys. Rev. A 3, 1849 (1971).

experimental data seems to support this hypothesis. The second assumption is based on known structures for other R-HX[22,25-29] compounds where R = acetylene or ethylene and X = Cl, F, CN. All of these complexes have T-shaped structures with the X → H vector perpendicular to and bisecting the π-bond. Since propyne does not have a plane of symmetry perpendicular to and bisecting the π-bond, a distorted T shaped structure is expected.

Figure 9. describes the structural parameters used to reproduce the effective rigid rotor rotational constants. The fitted values of these parameters are recorded in Table VII. It should be noted that these rotational constants are consistent with two possible T shaped structures, one in which the acid proton is located between the F-atom and the triple bond and another in which the hydrogen is on the opposite side of the F-atom, making it the farther atom of the two from the triple bond. Table IX clearly illustrates that only the former structure is consistent with the rotational constants of both propyne-HF and propyne-DF. An internal rotor analysis shall now be considered.

Table IX. Determination of HF Vector Directionality[a].

Assumed Structure	Fitted Distance to F (Å)
Propyne-HF	2.97
Propyne-DF	2.97
Propyne-FH	2.88
Propyne-FD	2.80

[a]For this purpose the FH vector was assumed to be perpendicular to, and bisect the propyne triple bond.

Figure 9.

The Principal Inertial Axes and Structural Parameters of Propyne-HF. Orthogonal zero-point bending modes result in a precessional motion and a vibrationally averaged quadrupole projection operator corresponding to the operationally-defined angle γ^* (see Equation 31).

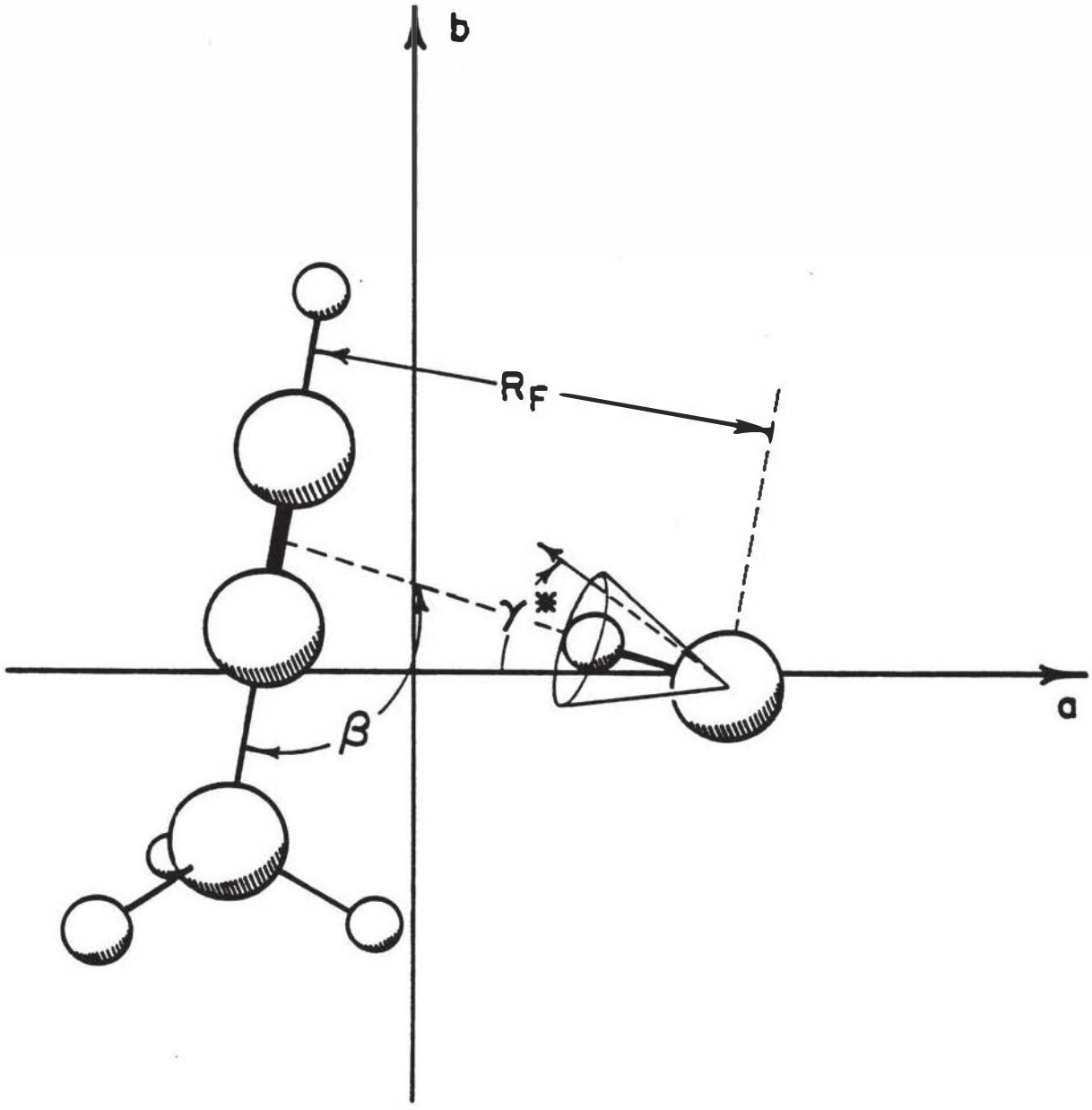
b
R_F
γ
β
a

It is of interest to qualitatively compare the observed propyne-HF/DF spectra with the corresponding transitions in methanol, which may be regarded as a well characterized near-prolate top which also exhibits a low C_3 barrier to internal rotation (see Figure 10). An accurate description of internal rotation must include coupling with the vibrational modes that affect the interaction of the methyl top with the neighboring atoms. Table X. shows that the rigid internal rotor Hamiltonian of equation 6, which totally neglects this coupling, fails to reproduce the quantitative torsional splittings. As expected, the A-symmetry lines are reproduced fairly well, but the calculated E symmetry lines are in poor agreement with the observed.

Table X. Comparision of the Rigid Internal-Rotor-Rigid Frame Spectrum of Methanol with the Observed.

	Measured[21]	Calculated	Resid
$0_{00} \rightarrow 1_{00}$ (A)	48377.09	48375.59	1.50
$1_{11} \rightarrow 2_{12}$ (A)	95914.29	95913.65	.64
$1_{01} \rightarrow 2_{02}$ (A)	96744.58	96745.25	-.67
$1_{10} \rightarrow 2_{11}$ (A)	97582.83	97582.07	.76
$0_{00} \rightarrow 1_{01}$ (E)	48372.60	48367.07	5.53
$1_{11} \rightarrow 2_{12}$ (E)	96755.51	96761.89	-6.38
$1_{01} \rightarrow 2_{02}$ (E)	96741.42	96726.50	14.92
$1_{10} \rightarrow 2_{11}$ (E)	96739.39	96734.58	4.81

Kirtman[30] has developed the theory of interaction of hindered internal rotation with ordinary vibration. However, this treatment requires the determination of eight parameters to describe a-dipole, R-branch transitions and 12 parameters to describe b-dipole, Q-branch

Figure 10.

Comparison of methanol (a), propyne-DF (b), and propyne-HF (c) spectra. Frequencies are in GHz.

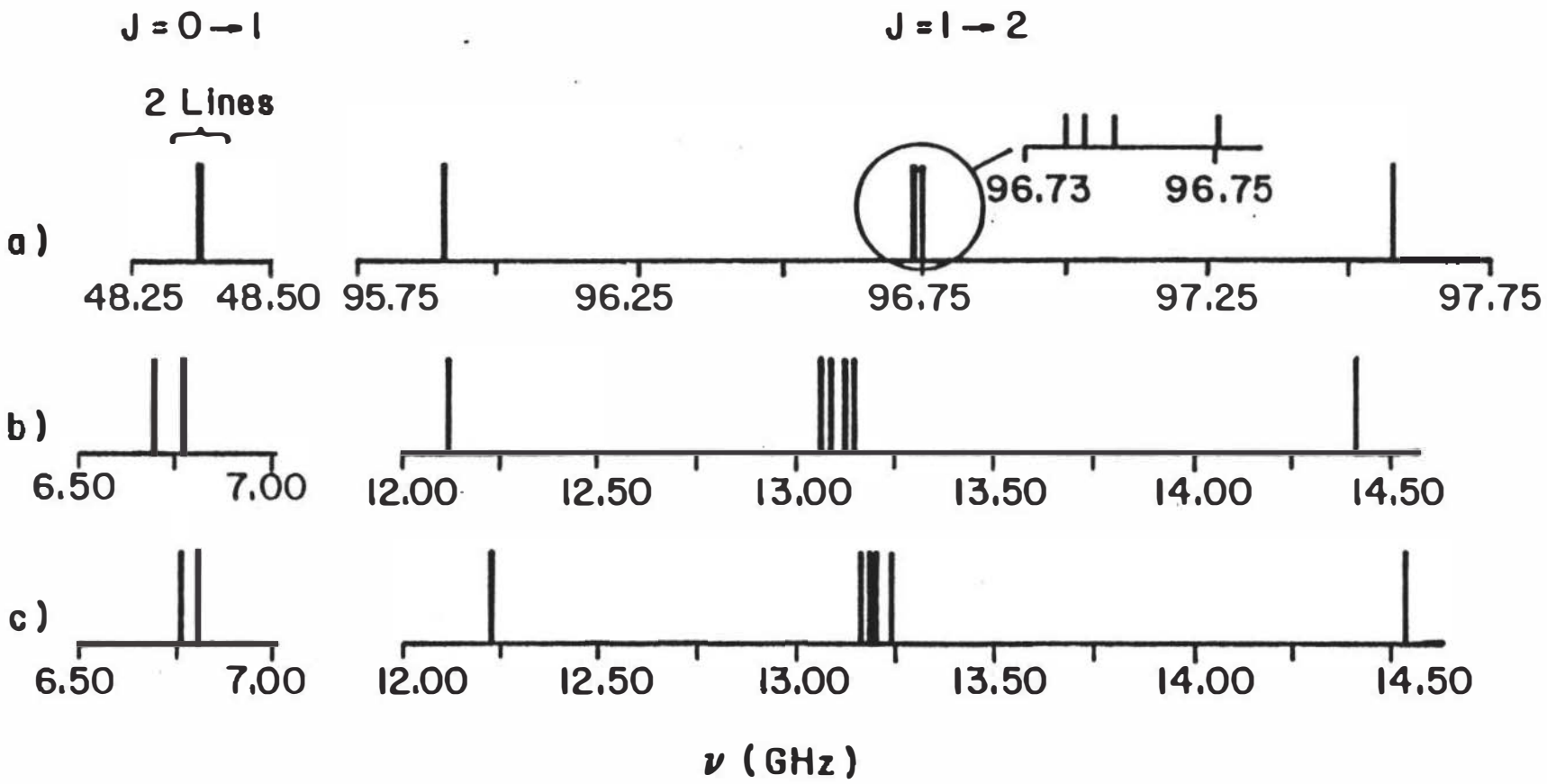
J = 0 → 1
J = 1 → 2
2 Lines
a)
b)
c)
48.25
48.50
95.75
96.25
96.73
96.75
96.75
97.25
97.75
6.50
7.00
12.00
12.50
13.00
13.50
14.00
14.50
6.50
7.00
12.00
12.50
13.00
13.50
14.00
14.50
ν (GHz)

transitions. Moreover, an accurate determination of the barrier can only be obtained if b-dipole, Q-branch transitions are observed. Lees and Baker[21] have succeeded in fitting all 20 of these parameters to several hundred methanol lines.

In view of the large amplitude, low frequency vibrational modes common to weakly bound complexes the need for including the interaction discussed above in describing propyne-HF is apparent. However, no Q-dipole transitions have been identified and only two a-dipole R-branches were observed in the experimentally accessible region. Thus the Hamiltonian described in equation 6 (the rigid rotor-rigid internal rotor) was applied. Although this treatment was not expected to reproduce the E symmetry lines, it is felt that the A symmetry lines and hence, the rotational constants derived from them are more accurately treated with this model.

In order to apply this model under these conditions, an estimate of the barrier height V_3 must be obtained. This was accomplished by fixing the rotational constants at values calculated from the effective rigid rotor structure averaged over both isotopic species and sweeping the barrier from 50-150 cm^{-1}. The results of this calculation are shown graphically in Figure 11. At barriers above 150 cm^{-1} the calculated spectrum approaches the high barrier limit of a harmonic librator with convergence to a rigid rotor spectrum, at barriers below 50 cm^{-1} torsional splittings are quite large. From the measured spectrum of propyne-HF plotted above the calculated spectrum, it is clear that 100 ±50 cm^{-1} is a reasonable estimate of the barrier.

Since the Hamiltonian matrix elements are sensitive to the direction cosines of the top axes with the principle axes which are in turn

Figure 11.

Calculated Spectrum of Propyne-HF as a Function of Barrier.

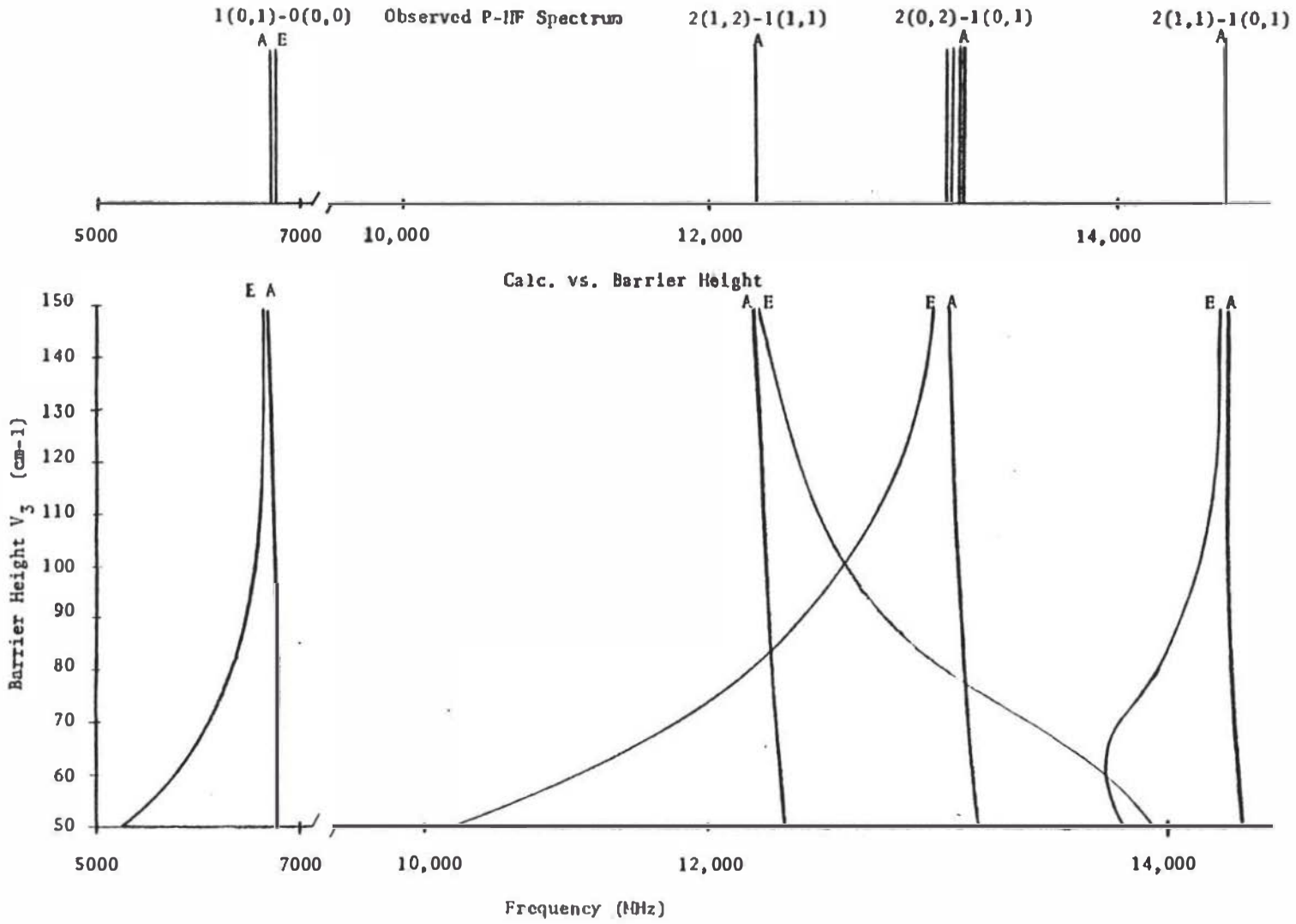
1(0,1)-0(0,0)
A E
Observed P-NF Spectrum
2(1,2)-1(1,1)
A
2(0,2)-1(0,1)
A
2(1,1)-1(0,1)
A
5000
7000
10,000
12,000
14,000
Calc. vs. Barrier Height
E A
A E
E A
E A
150
140
130
120
110
100
90
80
70
60
50
Barrier Height V_3 (cm-1)
5000
7000
10,000
12,000
14,000
Frequency (MHz)

dependent on the structure, it is convenient to fit the structural parameters defined in Figure 9 directly to the spectrum rather than to fit the rotational constants. A least squares fit of the A symmetry lines was carried out with V_3 fixed at 100 cm-1. The determined structural parameters are reported in Table V.

Although nuclear spin hyperfine splitting was observed for all lines, only the J=0-1 patterns were fully resolved and assigned (See Table XI). It can be shown that the J=0-1 hyperfine pattern is virtually independent of D_{bb}, D_{cc}, X_{bb}, X_{cc} and all the off diagonal elements of the coupling tensors. Hence, in principal, the J=0-1 splittings of propyne-HF should be calculable with the appropriate value of D_{aa} and likewise X_{aa} and D_{aa} for propyne-DF. However, only the J=0-1 pattern of propyne-DF could be reproduced by these calculations. This was accomplished by fitting X_{aa}, D_{aa} and a line center. The fitted values of X_{aa} and D_{aa} are recorded in Table VII and the calculated frequencies are recorded in Table X.

To interpret the values of X_{aa} and D_{aa} it is necessary to consider the expression

$$C = \tfrac{1}{2}C_o\langle 3\cos^2\gamma - 1\rangle \qquad (30)$$

giving the vibrationally averaged projection of the free DF spin-spin or deuterium quadrupole coupling constant C_o onto the a-axis of the complex where γ is the instantaneous angle the DF vector makes with the a-axis. An operationally defined angle corresponding to the vibrationally averaged value of this projection operator may then be defined,

$$\gamma^* = \arccos\left(\frac{2C}{3C_o} + 1/3\right)^{\frac{1}{2}} \qquad (31)$$

The values of γ^* calculated from D_{aa} and X_{aa} are recorded in Table VII.

Table XI. Nuclear Hyperfine Structure of the 0(0,0)-1(0,1) Transitions.

Propyne-HF					Propyne-DF					
I	F	I´	F´	Observed(MHz)	I	F	I´	F´	Observed(MHz)	Calc.(MHz)
1	1	1	1	6714.1762	3/2	3/2	3/2	3/2	6652.1558	6652.1560
0	0	0	1	6714.2204	1/2	1/2	1/2	3/2	6652.2229	6652.2258
1	1	1	2	6714.3025	3/2	3/2	3/2	5/2	6652.2354	6652.2321
1	1	1	0	6714.3277	3/2	3/2	3/2	3/2	6652.2746	6652.2735
					1/2	1/2	1/2	1/2	6652.2895	6652.2908

Discussion and Conclusion

The molecular structure of propyne-HF has been determined. The optimized structure has the acid proton of HF forming a hydrogen bond with the π-electron density of propyne and the F displaced towards the methyl group from a line perpendicular to and bisecting the propyne triple bond. This F displacement suggests the presence of a weak hydrogen bonding interaction between F and the methyl protons. This idea is further strengthened when one considers the van der Waals radii of fluorine and the methyl protons. As shown in Figure 12, the calculated coordinates for F place it in a position such that its van der Waals radius is nearly in contact with that of the nearest methyl proton, i.e., in the attractive region of the Lennard-Jones potential.

This attractive interaction between the F and the methyl protons may further suggest that minima in the internal rotation barrier potential occur when the methyl protons are eclipsed with F.

Due to the limited number of observed lines, the position of the proton of HF could not be given any degrees of freedom. Also, the rotational constants are not very sensitive to the position of this proton and hence, the constraint that the F → H vector bisects the triple bond was chosen. In view of the known structures of other π-complexes[22,25-29], this constraint seems reasonable. However, ab initio calculations indicate[34] that, in propyne, the charge density on the acetylenic carbon bonded to the methyl group is much smaller than the charge density on the other acetylenic carbon. Hence, it is likely that the chosen constraint on the position of the proton of HF places the proton too close to the methyl end of the triple bond of propyne.

Figure 12.

Van der Waals Contours of Propyne-HF.

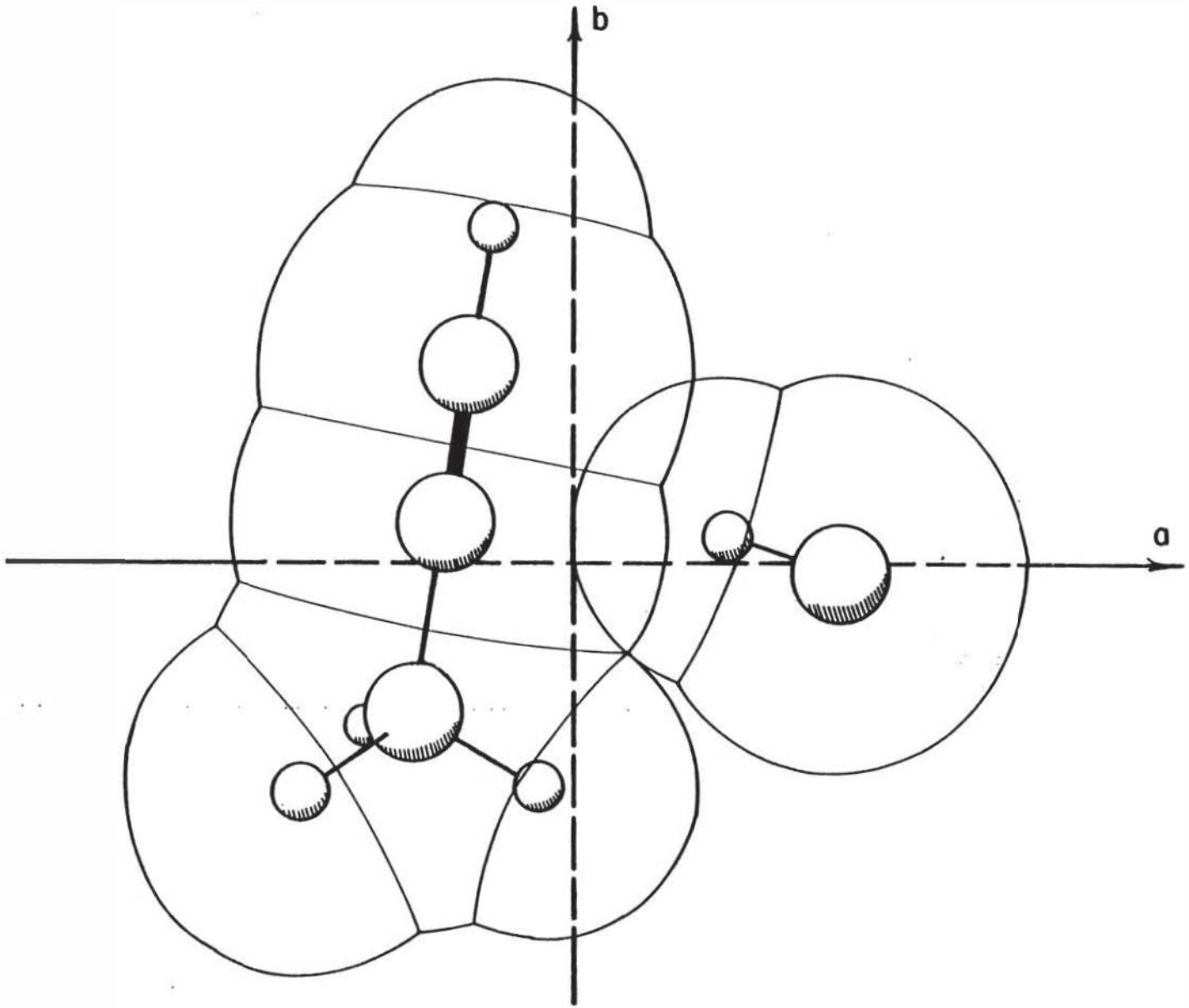
b
a

This study may represent the first example of rotational spectra which exhibit clear evidence of internal rotation in a van der Waals molecule. Rather large uncertainties in the spectroscopic constants are primarily due to model defects and cannot be improved upon without a significantly larger data set. However, the residuals of the calculated line centers are of the same order of magnitude as other internal rotor molecules done at this level of sophistication[35,36]. Figure 9 clearly indicates that the complex has a component of b-dipole and hence, as the sensitivity of experimental methods increases, b-dipole data may become available.

Table XII shows a comparison of barrier heights for several internal rotor molecules. From this table, one can identify certain qualitative trends in the dependence of barrier on structure. As expected, barrier height decreases as the distance of the internal tops protons from their nearest neighbor increases. This is demonstrated in the comparison of the barrier height of ethane with that of 2-butyne. Both molecules contain two axial methyl tops whose mutual interactions are responsible for the barrier to rotation. However, in 2-butyne the methyl groups are separated by a triple bond. As one can see, this decreases the barrier height by a factor of nearly 500. Another rather dramatic demonstration of this effect can be seen in the difference of barrier heights of cis- and trans- methyl nitrite. In trans-methyl nitrite, the N is the closest atom to the methyl protons whereas in cis-methyl nitrite, the O atom is in close proximity of the methyl protons resulting in a higher barrier.

It is also expected that barrier height depends on the number of nearest neighbors. This seems borne out in the series H_3COH, H_3CNH_2, H_3CCH_3. In these three molecules, the methyl protons interact with 1, 2 or 3 other protons approximately the same distance away on an sp^3 hybridized

Table XII. Barrier Heights of Selected Internal Rotor Molecules.

Formula	Name	$V_3(cm^{-1})$
H_3CONO	Trans-methyl nitrite[a.]	10
H_3CONO	Cis-methyl nitrite[a.]	731
H_3CCCCH_3	2-butyne[b.]	<2.1
H_3CCH_3	Ethane[c.]	1005
H_3CNH_2	Methylamine[d.]	692
H_2COH	Methanol[e.]	375.6
D_3COH	[e.]	371.8
H_3COD	[e.]	370.3
D_3CND_2	[a.]	684.7
H_3CCOF	Acetyl fluoride[d.]	363.8
H_3CCOCl	Acetyl chloride[d.]	453
H_3CCOBr	Acetyl bromide[d.]	456.1
H_3CCOI	Acetyl iodide[d.]	454.7
$H_3C\text{-}Cl_3$	Trichloro-ethane[d.]	1049
H_3COOOH	Peroxyacetic acid[f.]	76.7
$H_3CCOOCH_3$	Methyl acetate[f.]	99.6
H_3COOH	Acetic acid[g.]	167.8
H_3CCOCN	Acetyl cyanide[h.]	422.9

Table XII. (cont.)

a. Ref. 35.

b. Gordy, W. and Cook, R. L. Microwave Molecular Spectra, Interscience (1970).

c. Russell M. Pitzer, Acc. Chem. Res., 16, 207 (1983).

d. N.B.S. Monograph 70, Vol 3. "Microwave Spectral Tables, Polyatomic Molecules with Internal Rotation", U.S. Dept. of Commerce, Nat. Bur. of Standards (1969).

e. Ref. 24.

f. J. A. Cugley, W. Bossert, A. Bauder and Hs. H. Günthard, Chem. Phys. 16, 229 (1976).

g. L. C. Krisher and E. Saegebarth, J. Chem Phys., 54, 4553 (1971).

h. L. C. Krisher and E. B. Wilson, J. Chem. Phys. 31, 882 (1959).

center. The barriers to rotation for these molecules are 375.6, 692 and 1005 (cm^{-1}) respectively or roughly as 1:2:3 ratio. Also since the order of bond lengths is C-O<C-N<C-C, it is not surprising that the actual ratio is 1.12:2.07:3.

If one compares the barriers of deuterated species with those of non-deuterated species, the effect of vibrational interactions on barrier height is clearly observed. In general, substitution of an atom in the vicinity of or on the top, with a heavier isotope, results in a lowering of the barrier. This effect can be explained by recognizing that the barrier to internal rotation in a molecule depends upon the vibrationally averaged interaction of the top with the neighboring atoms. Isotopic substitution with a heavier atom lowers the vibrationally averaged displacement of that atom, usually resulting in a lower time averaged interaction and hence, a lower barrier. As discussed in the Method and Results section, this effect is particularly large in weakly-bound complexes. Indeed, the torsional splittings in the spectrum of propyne-DF are larger than those of propyne-HF (see Figure 10), suggesting a lower barrier for propyne-DF.

It is also of interest to compare the barrier heights of a homologous series such as H_3CCOX where X - F, Cl, Br or I. One would expect competing effects in progressing through this series. The interaction between the methyl protons and the halide would be expected to decrease as the electronegativity of the halide decreases, but should increase as the van der Waals radius of the halide increases. Apparently the size of the halide atom is most important as the barriers are 364, 453, 456 and 455 cm^{-1} respectively.

The optimized structure of propyne-HF compares favorably with other known π-complexes. As shown in Table XIII, the calculated distance from

Table XIII. Comparison of Bond Lengths of Propyne-HF and Some Other Weakly Bound Complexes.

	R(H) (Å)[a]
Propyne-HF	2.18
Acetylene-HF[b]	2.19
Ethylene-HF[c]	2.22
Benzene-HF[d]	2.25
Acetylene-HCl[e]	2.41
Ethylene-HCl[f]	2.44
Benzene-HCl[g]	2.35

[a] R(H) is distance from H of HX to the center of the π-bond or benzene center of mass.

[b] Ref. 25.

[c] Fre. 29.

[d] Ref. 37.

[e] Ref. 29.

[f] Ref. 30.

[g] Ref. 38.

the H of HF to the center of the triple bond of propyne fits well in the series R-HX where R = acetylene, ethylene and benzene and X = F or Cl. If shorter bond lengths are taken to indicate higher gas phase Lewis acidity, these complexes demonstrate the expected trend of HF<HCl.

Appendix 1.

Properties of Selected Weakly Bound Complexes.

Molecule	Point Group	De(kJ/mol)	$Re^{\dagger}$ (nm)	Method*	Ref.
Mg_2	$D_{\infty h}$	5.09	.389	hν	a
Ca_2	$D_{\infty h}$	13.0	.428	hν	a
Ne_2	$D_{\infty h}$	.350	.3102	DS,S	a
Ar_2	$D_{\infty h}$	1.185	.3761	DS,S,L,G	a
Kr_2	$D_{\infty h}$	1.684	.4007	DS,G,S,hν	a
Xe_2	$D_{\infty h}$	2.344	.4362	DS,G,S,hν	a
$Ne\text{-}H_2$	$C_{\infty v}$	.329	.344	SLR	a
$Ar\text{-}H_2$	$C_{\infty v}$	.691	.361	hν	a
$Kr\text{-}H_2$	$C_{\infty v}$	.829	.374	hν	a
$Xe\text{-}H_2$	$C_{\infty v}$	.918	.393	hν	a
Ar-HF	$C_{\infty v}$	1.4	.35	MBER	a
Ar-HCl	$C_{\infty v}$	1.5	.39	MBER	a
Ar-ClF	$C_{\infty v}$	2.7	.33	MBER	a
Kr-ClF	$C_{\infty v}$	3.4	.34	MBER	a
$Ar\text{-}N_2$	C_{2v}	$\geq$1.14	.39	DS,hν	a
$Ar\text{-}O_2$	C_{2v}	$\geq$1.23	.35	DS,hν	a
$(N_2)_2$	C_{2v}	.79	.37	hν,G	a
$(NO)_2$	C_{2v}	>6.7	$\geq$.18	hν	a
$(CO_2)_2$	C_{2v}	1.6	$\leq$.41	hν,G	a
ArOCS	C_s		$\geq$.35	MBER	a
H_2N_2	?	$\geq$.54	.35	hν,G	a
$H_3P\text{-}HF$	C_{3v}		.331	FB	b
$H_3P\text{-}HCl$	C_{3v}		.338	FB	c

Appendix 1. (cont.)

Molecule	Point Group	De(kJ/mol)	Re† (nm)	Method*	Ref.
H_3P-HBr	C_{3v}		.406	FB	d
H_3P-HCN	C_{3v}		.461	FB	e
C_2H_2-HF	C_{2v}		.307	FB	f
C_2H_2-HCl	C_{2v}	7.35	.366	FB	g
C_2H_2-HCN	C_{2v}	6.88	.421	FB	h
C_2H_4-HF	C_{2v}		.310	FB	i
C_2H_4-HCl	C_{2v}	6.88	.367	FB	j
C_2H_4-HCN	C_{2v}	6.88	.426	FB	k
C_3H_6-HF	C_{2v}	22.4	.312	FB	l
C_3H_6-HCL	C_{2v}	10.2	.370	FB	m
C_3H_6-HCN	C_{2v}	10.3	.447	FB	n
C_6H_6-HF	C_{6v}		.32	MBER	o
C_6H_6-HCl	C_{6v}	8.61	.36	FB	p
C_6H_6-Ar	C_{6v}		.34		q
Furan-Ar	C_s		.354	FB	r
Hq-HCl	$C_{\infty v}$		.410	FB	s
ArClCN	C_s		.364	FB	t

†Re is center of mass to center of mass distance.

*hν - absorption spectroscopy; DS = differential scattering; S, L and G correspond to bulk property measurements, solid, liquid, gas; MBER = molecular beam electron resonance; FB = Flygare-Balle Spectrometer; SLR = Spin Lattice Relaxation.

a. B. L. Blaney and G. E. Ewing, Ann. Rev. Phys. Chem., 27, 553-86 (1976).

b. A. C. Legon, J. Phys. Chem. 87, 2064 (1983).

c. A. C. Legon and L. C. Willoughby, Chem. Phys. 74, 127 (1983).

Appendix 1. (cont.)

d. L. C. Willoughby and A. C. Legon, J. Phys. Chem. 87, 2085 (1983).

e. A. C. Legon and L. C. Willoughby, to be published Chem. Phys. (1984).

f. Ref. 25.

g. Ref. 29.

h. P. D. Aldrich, S. G. Kukolich and E. J. Campbell, J. Chem. Phys. 78, 3521 (1983).

i. Ref. 28.

j. Ref. 30.

k. S. G. Kukolich, W. G. Read, and P. D. Aldrich, J. Chem. Phys., 78, 2552 (1983).

l. L. W. Buxton, P. D. Aldrich, J. A. Shea, A. C. Legon and W. H. Flygare, J. Chem. Phys., 75, 2681 (1981).

m. A. C. Legon, P. D. Aldrich and W. H. Flygare, J. Am. Chem. Soc. 104, 1486 (1982).

n. S. G. Kukolich, J. Chem. Phys. 78, 4832 (1983).

o. Ref. 37.

p. Ref. 38.

q. K. H. Fung, H. L. Selze and E. W. Schlag, Z. Naturforsh, A, 36, 1338 (1981).

r. S. G. Kukolich and J. A. Shea, J. Chem. Phys., 77, 5242 (1982).

s. E. J. Campbell and J. A. Shea to be published, J. Chem. Phys. (1983-84).

t. Ref. 27.

Appendix 2. Derivation of Internal Rotor Matrix Elements

To derive the Hamiltonian in the form of equation 6, one begins with

$$H = T+(V_m/2)(1-\cos m\alpha) \tag{A2-1}$$

where T is the total kinetic energy and the second term is the potential energy. The kinetic energy may be written[21]

$$T = \tfrac{1}{2}[\Sigma_g I_g w_g^2+2I_\alpha\dot{\alpha}\Sigma_g\lambda_g w_g+I_\alpha\dot{\alpha}^2] \tag{A2-2}$$

$$g = x,y,z.$$

where w_g is the component of angular velocity of the frame about the g-principal axis, I_g is the moment of inertia about the g-axis, I_α is the moment of inertia of the top about its symmetry axis and $\dot{\alpha}$ is the angular velocity of the top relative to the frame. The angular momenta are then defined by

$$J_g = \partial T/\partial w_g = I_g w_g+\lambda_g I_\alpha\dot{\alpha} \tag{A2-3}$$

$$p = \partial T/\partial\dot{\alpha} = I_\alpha\dot{\alpha}+I_\alpha\Sigma_g\lambda_g w_g. \tag{A2-4}$$

Hence, the components of total angular momentum J_g, contain a contribution from internal motion; and the total angular momentum of the internal top, p includes contributions from overall rotation. For a rigid rotor, T would be $\frac{1}{2}\Sigma_g J_g^2/I_g$. This term can be subtracted from the total kinetic energy to separate the rigid rotor Hamiltonian,

$$T=\tfrac{1}{2}\Sigma_g J_g^2/I_g = \tfrac{1}{2}[1-\Sigma_g\lambda_g^2 I_\alpha/I_g]I_\alpha\dot{\alpha}^2$$

$$\text{or} \qquad T = \tfrac{1}{2}[1-\Sigma_g\lambda_g^2 I_\alpha/I_g]I_\alpha\dot{\alpha}^2+\tfrac{1}{2}\Sigma_g J_g^2/I_g. \tag{A2-5}$$

The coefficient of $\dot{\alpha}^2$ is the reduced moment of inertia for internal rotation which will be denoted $2rI_\alpha$. The relative angular momentum of the internal top and framework may then be defined by

$$p-P = 2rI_\alpha\dot{\alpha} \tag{A2-6}$$

From A2-5 and A2-4 it is evident that

$$P = \sum_g J_g\lambda_g I_\alpha/I_g = \beta J_x+\gamma J_y+\alpha J_z \tag{A2-7}$$

where

$$\alpha = \frac{\lambda_z I_\alpha}{I_{zz}}, \qquad \beta = \frac{\lambda_x I_\alpha}{I_{xx}} \qquad \text{and } \gamma = \frac{\lambda_y I_\alpha}{I_{yy}},$$

where α, β and γ are choosen to correspond to A, B and C in the prolate basis.

Substitution of A2-6 into A2-5 yields,

$$T = H_{RR}+F(p-P)^2, \tag{A2-8}$$

where,

$$F = \frac{h^2}{2rI_\alpha} \tag{A2-9}$$

and H_{RR} is the usual rigid rotor Hamiltonian. Substitution of A2-8 into A2-1 yields,

$$H = H_{RR}+F(p-P)^2+(Vm/2)(1-\cos m\alpha). \tag{6}$$

If the second term in the Hamiltonian (equation 6) is expanded and the potential function is written as appropriate for a C_3 barrier, one obtains,

$$H = H_{RR}+Fp^2+FP^2-2FPp+(V_3/2)(1-\cos 3\alpha). \qquad \text{(A2-3)}$$

Since a low barrier was expected in this case, the matrix representation of the above Hamiltonian was written in the $|JKM_Jm\rangle$ basis, where J, K, and M_J pertain to the prolate symmetric rotor basis and m correpsonds to the free rotor basis, i.e. wave functions of the form $e^{im\alpha}$. In order to allow the barrier function to interact more favorably with the free rotor wave functions, the barrier function is written in the Euler form;

$$\text{Barrier} = (V_3/2)\ 1 - \frac{e^{i3\alpha}-e^{-i3\alpha}}{2}. \qquad \text{(A2-4)}$$

The matrix elements of equation A2-3 are most conviently derived term by term, the parts of which may be summed to yield H. Since the matrix elements of the rigid rotor prolate basis are diagonal in both J and M, the notation following will be shortened to $|km\rangle$ with $\delta_{JJ'}\delta_{MM'}$ understood.

The first term of equation A2-3 is the usual rigid rotor Hamiltonian with matrix elements given as follows,[19]

$$\langle K\ m|H_{RR}|k\ m'\rangle = \delta_{MM'}[h(B+C)/2][J(J+1)-K^2]+hK^2A \qquad \text{(A2-5)}$$

$$\langle K\ m|H_{RR}|K\pm2\ m'\rangle = \delta_{mm'}[h(B-C)/4][J(J+1)-K(K\pm1)]^{\frac{1}{2}}[J(J+1)-(K\pm1)K\pm2)]^{\frac{1}{2}}, \qquad \text{(A2-6)}$$

the $\delta_{mm'}$ coming from the fact the H_{RR} does not operate on the m space.

The matrix representation of Fp^2 can be written,

$$\langle K\ m|Fp^2|K'\ m'\rangle. \qquad \text{(A2-7)}$$

Since F is a constant and p does not operate on the K space,

$$\langle K\ m|Fp^2|k\ m'\rangle = \delta_{kk'}F\langle m|p^2|m'\rangle =$$

$$\delta_{kk'} F \int_0^{2\pi} e^{-im\alpha} \left[\frac{\partial^2}{\delta x^2}(e^{im'\alpha})\right]\delta\alpha = F\alpha_{kk'}\delta_{mm'}m^2. \qquad \text{(A2-8)}$$

The matrix representation of the third term of equation A2-3 is

$$\langle K\ m|FP^2|K',m'\rangle = F\langle Km|P^2|K'm'\rangle = F\langle K,m|P|K,m\rangle\langle K,m|P|K',m'\rangle \qquad \text{(A2-9)}$$

Recall that

$$P = \beta J_x + \gamma J_y + \alpha J_z. \qquad \text{(A2-2)}$$

Hence, we require the matrix representation of J_x, J_y and J_z, the x,y,z components of the rigid rotor angular momentum. For the prolate case, These are given as,[19]

$$\langle K|J_y|K\pm1\rangle = \mp(ih/2)\,[J(J+1)-K(K\pm1)]^{\frac{1}{2}} \qquad \text{(A2-10)}$$

$$\langle K|J_z|K\rangle = hK \qquad \text{(A2-11)}$$

$$\langle K|J_x|K\pm1\rangle = (h/2)\,[J(J+1)-K(K\pm1)]^{\frac{1}{2}}.$$

Therefore,

$$\langle K.m|P|K,m\rangle = K\alpha \qquad \text{(A2-13)}$$

$$\langle K\ m|P|K\pm1,m\rangle = [\beta\mp i\gamma)/2]\,[J(J+1)-K(K\pm1)]^{\frac{1}{2}}. \qquad \text{(A2-14)}$$

Hence, to obtain the matrix representation of P^2, one multiplies two tridiagonal matrices,

$$\langle K\ m|P^2|K',m'\rangle = \sum_{k'',m''}\langle K,m|P|K'',m''\rangle\langle K'',m''|P|K'm'\rangle. \qquad \text{(A2-15)}$$

This yields diagonals in K and off diagonals in K by ±1 and ±2 as follows:

Diagonals in K

$$\langle K,m|P^2|K,m\rangle = \langle K,m|P|K,m\rangle\langle K,m|P|K,m\rangle+\langle K-1,m|P|K,m\rangle\langle K,m|P|K-1,m\rangle+$$

$$\langle K+1,m|P|K,m\rangle\langle K,m|P|K+1,m\rangle = \alpha^2K^2+[(\beta-i\gamma)/2][J(J+1)-(K-1)K]^{\frac{1}{2}}[(\beta+i\gamma)/2]\cdot$$

$$[J(J+1)-K(K-1)]^{\frac{1}{2}}+[(\beta+i\gamma)/2][J(J+1)-(K+1)K]^{\frac{1}{2}}[(\beta-i\gamma)/2][J(J+1)-K(K+1)]^{\frac{1}{2}} =$$

$$\alpha^2K^2+[(\beta^2+\gamma^2)/2][J(J+1)-K^2] \qquad \text{(A2-16)}$$

Off diagonals in K by 1

$$\langle K,m|P^2|K\pm1,m\rangle = \langle K,m|P|K\pm1,m\rangle\langle K,m|P|k,m\rangle+\langle K\pm1,m|P|K\pm1,m\rangle\langle K,m|P|K\pm1km\rangle =$$

$$[(\beta+-i\gamma)/2][J(J+1)-K(K\pm1)]^{\frac{1}{2}}\alpha K+\alpha(K\pm1)[(\beta+-i\gamma)/2][J(J+1)-K(K\pm1)]^{\frac{1}{2}} =$$

$$\alpha(2K\pm1)[\beta+1i\gamma)/2)[J(J+1)-K(K\pm1)]^{\frac{1}{2}}$$

Off diagonals in K by 2

$$\langle K,m|P^2|K\pm2,m\rangle = \langle K\pm1|P|k\pm2\rangle\langle K|P|K\pm1\rangle = [(\beta+-i\gamma)/2][J(J+1)9(K\pm1)(K\pm2)]^{\frac{1}{2}}$$

$$[\beta+-i\gamma/2)][J(J+1)-K(K\pm1)]^{\frac{1}{2}} = [(\beta+-i\gamma)^2/4][J(J+1)-K(K\pm1)]^{\frac{1}{2}}$$

$$[J(J+1)-(K\pm1)(K\pm2)]^{\frac{1}{2}} \qquad \text{(A2-18)}$$

Hence from the third term of equation A2-3 one obtains

$$\langle K,m|FP^2|K,m\rangle = F\alpha^2K^2+[F(\beta^2+\gamma^2)/2][J(J+1)-K^2] \qquad \text{(A2-19)}$$

$$\langle K,m|FP^2|K\pm1,m\rangle = F\alpha(2K\pm1)[(\beta+-i\gamma)/2][J(J+1)-K(K\pm1)]^{\frac{1}{2}} \qquad \text{(A2-20)}$$

$$\langle K,m|FP^2|K\pm2,m\rangle = [F(\beta+-i\gamma)^2/4][J(J+1)-K(K\pm1)]^{\frac{1}{2}}[J(J+1)-(K\pm1)(K\pm2)]^{\frac{1}{2}}. \quad (A2\text{-}21)$$

The fourth term in equation A2-3 is represented as

$$\langle K,m|-2Pp|K',m'\rangle = -2F\langle K|P|K'\rangle\langle m|p|m'\rangle \quad (A2\text{-}22)$$

where the above separation is possible because P and p operate on the K and m coordinates respectively.

$$-2F\langle K|P|K'\rangle\langle m|p|m\rangle = -2F\langle K|P|K'\rangle\int_0^{2\pi} e^{-im\alpha}(\partial/\partial\alpha e^{im\alpha}]\partial\alpha = -2Fm\ K|P|K' \quad (A2\text{-}23)$$

Substituting equations (A2-13) and (A2-14) into (A2-23) one obtains,

$$\langle K,m|-2FPp|K,m\rangle = -2FmK\alpha \quad (A2\text{-}24)$$

and

$$\langle K,m|-2FPp|K\pm1,m\rangle = -2Fm[(\beta+-i\gamma)/2][J(J+1)-K(K\pm1)]^{\frac{1}{2}}. \quad (A2\text{-}25)$$

The final term of equation (A2-3) is

$$\langle K,m|(V_3/2)\left(1-\frac{e^{i3\alpha}-e^{-i3\alpha}}{2}\right)|K'm'\rangle =$$

$$\delta_{kk'}V_3/2\int_0^{2\pi}[e^{-im\alpha}\left(1-\frac{e^{i3\alpha}-e^{-i3\alpha}}{\quad}\right)e^{im\alpha}]\delta\alpha =$$

$$\delta_{KK'}\delta_{mm'}(V_3/2) \quad \text{and}$$

$$\delta_{KK'}\delta_{mm\pm3}(-V_3/4). \quad (A2\text{-}26)$$

Hence,

$$\langle Km|(V_3/2)(1-\cos3\alpha)|Km\rangle = V_3/2 \quad (A2\text{-}27)$$

$$\langle Km|V_3/2)\,(1-\cos 3\alpha)\,|Km\pm 3\rangle = -V_3/4 \qquad \text{(A2-28)}$$

To obtain $\langle Km|H|K'm'\rangle$ one sums up the above derived parts yielding

$$\langle K,m|H|k,m\rangle = [(B+C+F\beta^2+F\gamma^2)/2][J(J+1)-K^2]+(\alpha^2F+A)K^2+$$

$$Fm^2-2Fm\alpha K+V_3/2 \qquad (10)$$

$$\langle K,m|H|Km\pm 3\rangle = -V_3/4 \qquad (11)$$

$$\langle K,m|H|K\pm 1,m\rangle = (F/2[\alpha(2K\pm 1)-2m](\beta+-i\gamma)[J(J+1)-K(K\pm 1)]^{\frac{1}{2}} \qquad (12)$$

$$\langle K,m|H|K\pm 2,m\rangle = \{[C-B+F(\beta+-i\gamma)^2]/4\}[J(J+1)-K(K\pm 1)]^{\frac{1}{2}}[J(J+1)-(K\pm 1)(K\pm 2)]^{\frac{1}{2}}, \qquad (13)$$

where the above expressions are understood to be in frequency units.

Appendix 3.

Jacobi Least Squares Fitting Program.

```
00100  PROGRAM JACOB(INPUT,OUTPUT,DATA,TAPE5=INPUT,TAPE6=OUTPUT,
00110+TAPE7=DATA)
00120C   PROGRAM TO PERFORM GENERAL JACOBIAN LEAST SQUARES FITS
00130C   WRITTEN BY ROGER BUMGARNER, JAN., 1983.
00140C   BASED ON ALGORITM FROM HYUNYONG KIM, J. CHEM. ED.,VOL.47,
00150C   PGS. 120-122,(1970).
00160C   PROGRAM REQUIRES TWO SUBROUTINES, "FSUB", AND "OUTPUT".
00170C   "FSUB" IS A SUBROUTINE WHICH IS PASSED PARAMETERS (VECTOR
00180C   "ALPHA") AND RETURNS CALCULATED VALUES OF THE FUNCTION (VECTOR
00190C   "Y     ")."MDIM" IS THE DIMENSION OF THE MATRICES IN THE MAIN
00200C    PROGRAM AND MAY, OF COURSE, BE CHANGED TO SUIT ONE'S NEEDS.
00210C    "NDPTS" AND "NPARMS" ARE THE NUMBER OF DATA PTS. AND PARAMETERS
00220C    RESPECTIVELY. THESE MAY OR MAY NOT BE NEEDED BY "FSUB" BUT ARE
00230C    PASSED FOR GENERAL COMPATABILITY. "OUTPUT" IS A USER WRITTEN
00240C    SUBROUTINE TO GENERATE THE THE DESIRED OUTPUT FORMAT."OUTPUT"
00250C    IS CALLED ON EACH ITERATIVE CYCLE."OUTPUT" IS PASSED "MDIM",
00260C    "NDPTS" AND "NPARMS" AS IS "FSUB". IT IS ALSO PASSED "DATA"-
00270C    A VECTOR CONTAINING THE DATA WHICH IS BEING FIT,"YOUGHT"-THE
00280C    CALCULATED VALUES FOR THIS SET OF PARAMETERS,"ALPHA"-THE FITTED
00290C    SET OF PARAMETERS,"KOUNT"-THE # OF THE ITERATIVE CYCLE,"SS"-THE
00300C    VARIANCE OF THE OVERALL FIT,"V"-A VECTOR CONTAINING THE VARIANCE
00310C    EACH PARAMETER "ALPHA",AND "KV"-A SWITCH TO INDICATE WHETHER
00320C    OR NOT TO OUTPUT "V". "KV"=0 ON THE ZERO'TH ORDER SWEEP SINCE
00330C    "V" CANNOT YET BE CALCULATED, THEREAFTER KV=1 I.E. OUTPUT "V".
00340C    STATEMENT 81 IS A GENERAL PURPOSE TITLE FORMAT TO BE CHANGED
00350C    FOR EACH TYPE OF RUN. DATA READ BY THE MAIN PROG. IS "NDPTS",
00360C    "NPARMS","DATA" AND "ALPHA" (INITIAL GUESSES). THE CHOSEN
00370C    CRITERIA FOR CONVERGENCE IS THAT THE VARIANCE OF THE OVERALL FIT
00380C    OF A GIVEN CYCLE IS NOT LESS THAN THE OLD VAR. - 1E-5*(OLD VAR.)
00390C    OR SIX ITERATIVE CYCLES.
00400       DIMENSION DATA(20),ALPHA(20),ALPHA2(20),YOUGHT(20),YPRIME(20)
00410       DIMENSION RJACOB(20,20),EVECT(20,20),C(20,20),DELTAA(20,20)
00420       DIMENSION TRNSPJ(20,20),TE(20,20),V(20),ASAVE(20),DSAVE(20)
00430       MDIM=20
00440       KOUNT=0
00450       SSOLD=1.0E16
00460       KV=0
00470       ICON=0
00480C**************INITIALIZATION**********************************
00490       W=0.0
00500       DO 3 I=1,20
00510          DATA(I)=W
00520          ALPHA(I)=W
00530          ALPHA2(I)=W
00540          YOUGHT(I)=W
00550          YPRIME(I)=W
00560          V(I)=W
00570          DO 2 J=1,20
00580             RJACOB(I,J)=W
00590             DELTAA(I,J)=W
00600             EVECT(I,J)=W
00610             C(I,J)=W
00620             TRNSPJ(I,J)=W
00630             TE(I,J)=W
00640     2    CONTINUE
```

```
00650    3 CONTINUE
00660C*************************************************************
00670C  READ NUMBER OF DATA PTS. AND PARAMETERS
00680      READ(7,1)NDPTS,NPARMS
00690      WRITE(6,31)NDPTS,NPARMS
00700C  READ AND ECHO DATA
00710      DO 10 I=1,NDPTS
00720         READ(7,11)DATA(I)
00730         WRITE(6,41)I,DATA(I)
00740   10 CONTINUE
00750C  READ AND AND ECHO PARAMETER GUESSES
00760      DO 20 I=1,NPARMS
00770         READ(7,11)ALPHA(I)
00780         WRITE(6,51)I,ALPHA(I)
00790   20 CONTINUE
00800C  CALCULATE YOUGHT
00810   25 CALL FSUB(MDIM,NDPTS,NPARMS,ALPHA,YOUGHT)
00820      DO 40 J=1,NPARMS
00830         DELAL=ALPHA(J)*1.0E-6
00840C  GIVE DELAL SMALL FINITE VALUE IF ALPHA(J)=0
00850         IF(DELAL.EQ.0.0)DELAL=1.0E-6
00860         DO 30 I=1,NPARMS
00870            ALPHA2(I)=ALPHA(I)
00880            IF(I.EQ.J)ALPHA2(I)=ALPHA(I)+DELAL
00890   30    CONTINUE
00900C CALCULATE YPRIME
00910         CALL FSUB(MDIM,NDPTS,NPARMS,ALPHA2,YPRIME)
00920C CALCULATE JACOBIAN MATRIX
00930         DO 35 I=1,NDPTS
00940            RJACOB(I,J)=(YPRIME(I)-YOUGHT(I))/DELAL
00950   35    CONTINUE
00960   40 CONTINUE
00970C CALCULATE ERROR VECTOR
00980      DO 50 I=1,NDPTS
00990         EVECT(I,1)=DATA(I)-YOUGHT(I)
01000   50 CONTINUE
01010C CALCULATE JACOBIAN'S TRANSPOSE
01020      DO 70 I=1,NDPTS
01030         DO 60 J=1,NPARMS
01040            TRNSPJ(J,I)=RJACOB(I,J)
01050   60    CONTINUE
01060   70 CONTINUE
01070C DO PRESCRIBED MATRIX OPERATIONS
01080      CALL MMULT(MDIM,NPARMS,NDPTS,NPARMS,TRNSPJ,RJACOB,C)
01090      CALL MTRXIN(MDIM,C,NPARMS)
01100      CALL MMULT(MDIM,NPARMS,NDPTS,1,TRNSPJ,EVECT,TE)
01110      CALL MMULT(MDIM,NPARMS,NPARMS,1,C,TE,DELTAA)
01120CSSSSS CALCULATE VARIANCE OF OVERALL FITSSSSSSSSSSSSSSSS
01130      SS=0.0
01140      DO 75 I=1,NDPTS
01150         SS=SS+(DATA(I)-YOUGHT(I))**2
01160   75 CONTINUE
01170      SS=SS/(NDPTS-NPARMS)
01180CSSSSSSSSSSSSSSSSSSSSSSSSSSSSSSSSSSSSSSSSSSSSSSSSSSSSSSSS
01190C CHECK FOR DIVERGENCE IF SO ATTEMPT DAMPENED FIT
```

```
01200      IF(SS.GT.SSOLD)GO TO 190
01210C RESET NO DIVERGENCE SWITCH
01220      ICON=0
01230      SR=SSOLD-SSOLD*1.0E-5
01240C CHECK FOR CONVERGENCE
01250      IF(SS.GT.SR)GO TO 200
01260      SSOLD=SS
01270      CALL OUTPUT(MDIM,NDPTS,NPARMS,DATA,YOUGHT,ALPHA,KOUNT,SS,V,KV)
01280      DO 80 I=1,NPARMS
01290         ASAVE(I)=ALPHA(I)
01300         DSAVE(I)=DELTAA(I,1)*0.1
01310         ALPHA(I)=ALPHA(I)+DELTAA(I,1)
01320   80 CONTINUE
01330C CALCULATE DIAGS OF VARIANCE-COVARIANCE MATRIX
01340      DO 100 I=1,NPARMS
01350         V(I)=SS*C(I,I)
01360  100 CONTINUE
01370      KV=1
01380C CHECK FOR TOO MANY ITERATIONS
01390      IF(KOUNT.GT.5)GO TO 200
01400      KOUNT=KOUNT+1
01410      GO TO 25
01420C CHECK TO SEE IF DAMPENED FIT HAS PREVIOUSLY BEEN ATTEMPTED ON
01430C THIS ITERATIVE CYCLE
01440  190 IF(ICON.GT.0)GO TO 195
01450      WRITE(6,71)
01460      DO 192 I=1,NPARMS
01470         ALPHA(I)=ASAVE(I)+DSAVE(I)
01480  192 CONTINUE
01490      ICON=1
01500      GO TO 25
01510  195 WRITE(6,21)
01520      STOP
01530  200 CONTINUE
01540C OUTPUT FINAL JACOBIAN MATRIX
01550      CALL OUTPUT(MDIM,NDPTS,NPARMS,DATA,YOUGHT,ALPHA,KOUNT,SS,V,KV)
01560      DO 350 I=1,NPARMS
01570         DO 300 J=1,NDPTS
01580            WRITE(6,61)DATA(J),ALPHA(I),RJACOB(J,I)
01590  300    CONTINUE
01600  350 CONTINUE
01610      STOP
01620    1 FORMAT(2I3)
01630   11 FORMAT(F20.4)
01640   21 FORMAT(1X,'ROUTINE IS NOT CONVERGING-TERMINATED')
01650   31 FORMAT(1X,'NDPTS=',I3,5X,'NPARMS=',I3)
01660   41 FORMAT(1X,'I=',I3,5X,'DATA(I)=',F20.4)
01670   51 FORMAT(1X,'I=',I3,5X,'ALPHA(I)=',F20.4)
01680   61 FORMAT(1X,' DATA PT ',F20.10,3X,'PARAMETER',
01690+     F20.10,3X,'SENSITIVITY',F20.10)
01700   71 FORMAT(1X,'***CAUTION]***ATTEMPTING DAMPENED FIT')
01710      END
01720C*************************************************
01730      SUBROUTINE MMULT(MDIM,NAR,NAC,NBC,A,B,C)
01740C*************************************************
```

```
01750       DIMENSION A(MDIM,MDIM),B(MDIM,MDIM),C(MDIM,MDIM)
01760       DO 500 I=1,NAR
01770          DO 500 J=1,NBC
01780             C(I,J)=0.0
01790             DO 500 K=1,NAC
01800                C(I,J)=C(I,J)+A(I,K)*B(K,J)
01810   500 CONTINUE
01820       RETURN
01830       END
01840C*******************************************************
01850       SUBROUTINE MTRXIN(MDIM,A,N)
01860C*******************************************************
01870       DIMENSION A(MDIM,MDIM),IPV(50,3)
01880C    INITIALIZATION
01890       DO 1 J=1,N
01900     1 IPV(J,3)=0
01910C    SEARCHFOR PIVOT ELEMENT
01920       DO 3 I=1,N
01930          AMAX=0.0
01940          DO 6 J=1,N
01950             IF(IPV(J,3)-1)7,6,7
01960     7       DO 5 K=1,N
01970                IF(IPV(K,3)-1)9,5,9
01980     9          IF(AMAX-ABS(A(J,K)))11,5,5
01990    11 IROW=J
02000                ICOLUM=K
02010                AMAX=ABS(A(J,K))
02020     5       CONTINUE
02030     6 CONTINUE
02040       IPV(ICOLUM,3)=IPV(ICOLUM,3)+1
02050       IPV(I,1)=IROW
02060       IPV(I,2)=ICOLUM
02070C    INTERCHANGE ROWS TO PUT PIVOT ELEMENT ON DIAGONAL
02080       IF(IROW-ICOLUM)16,17,16
02090    16 DO 20 L=1,N
02100          SWAP=A(IROW,L)
02110          A(IROW,L)=A(ICOLUM,L)
02120    20 A(ICOLUM,L)=SWAP
02130C     DIVIDE PIVOT ROW BY PIVOT ELEMENT
02140    17 PIVOT=A(ICOLUM,ICOLUM)
02150       A(ICOLUM,ICOLUM)=1.0
02160       DO 23 L=1,N
02170    23 A(ICOLUM,L)=A(ICOLUM,L)/PIVOT
02180C     REDUCE THE NON PIVOT ROWS
02190       DO 3 L1=1,N
02200          IF(L1-ICOLUM)26,3,26
02210    26    T=A(L1,ICOLUM)
02220          A(L1,ICOLUM)=0.0
02230          DO 29 L=1,N
02240    29    A(L1,L)=A(L1,L)-A(ICOLUM,L)*T
02250     3 CONTINUE
02260C    INTERCHANGE THE COLUMNS
02270       DO 31 I=1,N
02280          L=N-I+1
02290       IF(IPV(L,1)-IPV(L,2))34,31,34
```

```
02300    34    JROW=IPV(L,1)
02310          JCOLUM=IPV(L,2)
02320          DO 32 K=1,N
02330             SWAP=A(K,JROW)
02340             A(K,JROW)=A(K,JCOLUM)
02350             A(K,JCOLUM)=SWAP
02360    32    CONTINUE
02370    31 CONTINUE
02380       RETURN
02390       END
02400C*************************************************
02410         SUBROUTINE OUTPUT(MDIM,NDPTS,NPARMS,DATA,Y,ALPHA,KOUNT,SS,V,KV)
02420C*************************************************
02430 DIMENSION DATA(MDIM),Y(MDIM),ALPHA(MDIM),V(MDIM)
02440 IF(KV.EQ.0)WRITE(6,81)
02450 WRITE(6,1)KOUNT
02460 DO 10 I=1,NPARMS
02470    IF(KV.EQ.0)WRITE(6,11)I,ALPHA(I)
02480    SD=SQRT(V(I))
02490    IF(KV.GT.0)WRITE(6,21)I,ALPHA(I),SD
02500 10 CONTINUE
02510 WRITE(6,31)SS
02520 DO 20 I=1,NDPTS
02530    RESID=DATA(I)-Y(I)
02540 20 WRITE(6,41)DATA(I),Y(I),RESID
02550 RETURN
02560 1 FORMAT(1X,'************************************************************'
02570+//,'  ITERATIVE CYCLE # ',I2//)
02580 11 FORMAT(1X,'PARAMETER(',I2,')= ',F20.10)
02590 21 FORMAT(1X,'PARAMETER(',I2,')= ',F20.10,'  SD= ',F20.10)
02600 31 FORMAT(//1X,'VARIANCE OF OVERALL FIT=  ',F30.10//)
02610 41 FORMAT(1X,'DATA=',F20.10,'    CALC=',F20.10,'    RESID=',F20.10)
02620 81 FORMAT(1H1,//1X,'PUT YOUR TITLE HERE'//)
02630 END
```

References

1. T. J. Balle and W. H. Flygare, Rev. Sic. Instrum., 52, 33 (1981).

2. George E. Ewing, Acc. Chem. Res., 8, 195 (1975).

3. Benjamin L. Blaney and George E. Ewing, Ann. Rev. Phys. Chem., 27, 553 (1976).

4. George E. Ewing, Angew. Chem. Int. Ed. Engl. 11, 486 (1972).

5. William Klemperer, Ber. Bunsenges, 78, 128 (1974).

6. George C. Pinentell, "The Hydrogen Bond", W.H. Freeman, San Fran. (1980).

7. A. C. Legon, J. Phys. Chem., 87, 2064 (1983).

8. R. D. Green, "Hydrogen Bonding in CH Groups", Wiley, N.Y. (1974).

9. Gary L. Johnson and Lester Andrews, J. Am. Chem. Soc., 102, 5739 (1980).

10. Gary L. Johnson and Lester Andrews, J. Am. Chem. Soc., 105, 163 (1983).

11. Stephen A. McDonald, Gary L. Johnson, Brian W. Keelan and Lester Andrews, J. Am. Chem. Soc., 102, 2892 (1980).

12. T. R. Dyke and J. S. Muenter, "International Review of Sciences, Phys. Chem. Ser. 2", Vol. 2, A. D. Buckingham Ed., Butterworths, London p. 27 (1975).

13. T. R. Dyke, B. J. Howard and W. Klemperer J. Chem. Phys., 56, 2442 (1972).

14. E. J. Campbell, L. W. Buxton, T. J. Balle, M.R. Keenan and W. H. Flygare, J. Chem. Phys. 74, 829 (1981).

15. E. J. Campbell, L. W. Buxton, T. J. Balle and W. H. Flygare, J. Chem. Phys., 74, 813 (1981).

16. T. J. Balle, E. J. Campbell, M. R. Keenan and W. H. Flygare, J. Chem. Phys., 72, 922 (1980).

17. W. G. Read, and E. H. Campbell, Phys. Rev. Lett. 49, 1146 (1982).

18. E. J. Campbell, W. G. Read and J. A. Shea, Chem. Phys. Lett. 94, 69 (1983).

19. W. H. Flygare, "Molecular Structure and Dynamics", Prentice Hall, Englewood Cliffs, New Jersey (1978).

20. G. W. King, R. M. Hainer and P. C. Cross, J. Chem. Phys., 11, 27 (1943).

21. B. L. Crawford, J. Chem. Phys., 8, 273 (1940).

22. D. L. Herschbach, J. Chem. Phys., 31, 91 (1959).

23. R. G. Lett and W. H. Flygare, J. Chem. Phys. 47, 4730 (1967).

24. R. M. Lees and J. G. Baker, J. Chem. Phys. 48, 5299 (1968).

25. W. G. Read and W. H. Flygare, J. Chem. Phys. 76, 2238 (1982).

26. N. F. Ramsey, "Molecular Beams", p. 80 Oxford University Press, London (1956).

27. M. R. Keenan, D. B. Wozniak and W. H. Flygare, J. Chem. Phys., 75, 631 (1981).

28. J. A. Shea and W. H. Flygare, J. Chem. Phys. 76, 4857 (1982).

29. A. C. Legon, P. D. Aldrich and W. H. Flygare, J. Chem. Phys. 75, 625 (1981).

30. P. D. Aldrich, A. C. Legon, and W. H. Flygare, J. Chem. Phys. 75, 2126 (1981).

31. P. D. Aldrich, J. G. Kukolich and E. J. Campbell, J. Chem. Phys. 78, 3521 (1983).

32. S. G. Kukolich, W. G. Read and P. D. Aldrich, J. Chem. Phys., 78, 3552 (1983).

33. B. Kirtman, J. Chem. Phys. 37, 2516 (1962).

34. Alan C. Hopkinson, Min H. Lieu, Keith Yates, Paul G. Mezey and Imre G. Csizmadia, J. Chem. Phys., 67, 517 (1977).

35. Paul H. Turner, Michael J. Corkbill and A. Peter Cox, J. Phys. Chem., 83, 1473 (1979).

36. E. V. Ivash and D. M. Dennison, J. Chem. Phys., 21, 1804 (1953).

37. F. A. Baiocchi, J. H. Williams and W. Klemperer, J. Phys. Chem. 87, 2079 (1983).

38. W. G. Read, E. J. Campbell and Giles Henderson, J. Chem. Phys. 75, 625 (1981).